Optical and proton magnetic resonance study of copper (II) acetate dimeric molecules in acetonitrile/acetic acid mixtures
by Jennie Li-Ming Wang Dirks

A thesis submitted in partial fulfillment of the requirements for the degree Of MASTER OF SCIENCE in Chemistry
Montana State University

Abstract:
NMR line width and line shift of the acidic proton of HAc, and the methyl protons of the acetic acid and acetonitrile in CH.COOH/CH CH solutions with and without copper acetate have been 33 measured between -45°C to 37°C with a few measurements at higher temperature. The results, indicate an acid proton exchange between acetic acid monomer and dimer, axial ligand exchange of both acetic acid and acetonitrile on the copper acetate dimeric molecules at all temperatures. In addition, at higher temperatures there is exchange of acetate between acetic acid and the bridging ligands of the copper acetate dimer, with an activation energy of the order of 10 Kcal mol-1

STATEMENT OF PERMISSION TO COPY

In presenting this thesis in partial fulfillment of the requirements for an advanced degree at Montana State University, I agree that the Library shall make it freely available for inspection. I further agree that permission for extensive copying of this thesis for scholarly purposes may be granted by my major professor, or, in his absence, by the Director of Libraries. It is understood that any copying or publication on this thesis for financial gain shall not be allowed without my written permission.

Jennie Wang Dirks

Name

Dec. 4 1975

Date

TO

my great husband

OPTICAL AND PROTON MAGNETIC RESONANCE STUDY OF COPPER(II) ACETATE DIMERIC MOLECULES IN ACETONITRILE/ACETIC ACID MIXTURES

by

JENNIE WANG DIRKS

A thesis submitted in partial fulfillment
of the requirements for the degree

of

MASTER OF SCIENCE

in

Chemistry

Approved:

Reed Howald
Chairman, Examining Committee

E. W. Anacker
Head, Major Department

Henry L. Parsons
Graduate Dean

MONTANA STATE UNIVERSITY
Bozeman, Montana

December, 1975

ACKNOWLEDGMENTS

I wish to express my appreciation to the faculty of the Department of Chemistry for their faith in me as a graduate student and for their financial support through teaching and research assistantships.

To Dr. Mundy and his research group who helped me in many ways, I wish to extend thanks. Especially I thank Dr. Reed A. Howald and his wife, Elaine, for with their prayers, guidance and assistance I got this work done.

To my parents and church, who provided for my education by their sacrifices and prayer, I am thankful.

TABLE OF CONTENTS

LIST OF TABLES

LIST OF FIGURES

ABSTRACT

NMR line width and line shift of the acidic proton of HAc, and the methyl protons of the acetic acid and acetonitrile in CH_3COOH/CH_3CH solutions with and without copper acetate have been measured between -45°C to 37°C with a few measurements at higher temperature. The results indicate an acid proton exchange between acetic acid monomer and dimer, axial ligand exchange of both acetic acid and acetonitrile on the copper acetate dimeric molecules at all temperatures. In addition, at higher temperatures there is exchange of acetate between acetic acid and the bridging ligands of the copper acetate dimer, with an activation energy of the order of 10 Kcal mol^{-1}.

INTRODUCTION

Copper Acetate

There are a number of good reviews[1] on the chemistry of copper. Copper(II) acetate is a typical transition metal compound, showing paramagnetism and color due to the presence of partially filled d orbitals. Copper(II) has a d^9 configuration. The $t_{2g}^6 e_g^3$ configuration expected for octahedral d^9 complexes is subject to a Jahn-Teller distortion. In most Cu(II) complexes this leads four shorter and stronger bonds which are roughly in a plane, and two weaker longer axial bonds. This causes further splitting of the d orbitals as described in Appendix D.

In solution in most organic solvents and in crystalline $Cu_2(CH_3COO)_4.2H_2O$ copper acetate exists as a binuclear complex in which the copper (II) ions are bridged by four acetate groups. This dimer has two axial positions available for weaker bonding of solvent or water molecules. The dimer structure is shown in Figure 1. In the crystal the copper (II) ions are 0.22 Å out of the plane of the four acetate oxygen atoms at a distance of 1.97 Å. The distance to the axial ligands is 2.20 Å. One striking feature of this structure is the close approach of the two copper (II) ions, 2.64 Å, which is only slightly greater than the interatomic distance in metallic copper, 2.56 Å. At this distance metal - metal bonding can be strong or weak, and may have multiple character.[2] In this case the interaction is

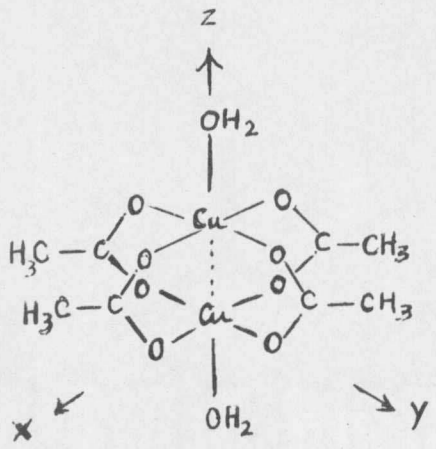

Figure 1. Schematic expression of the structure of $Cu_2(CH_3COO)_4.2H_2O$ molecule

antiferromagnetic as shown by the magnetic susceptibility[3-5] and by the paramagnetic resonance spectra.[6-13] There is also evidence on the nature of the bonding from the uv-visible spectrum, from the crystal structure,[14,15] and the temperature variation of the magnetic susceptibilities.[16-18] These are discussed more fully in Appendix D, however the full explanation of the nature of the copper-copper bond is still an interesting unsolved problem.[19-20]

Copper acetate exists mainly in the dimeric form in acetic acid and many other solvents.[21-26] The dimer spectrum is similar to that of copper acetate crystals with strong absorbance around 700 nm. There have been many attempts to interpret the dimer spectrum,[27-34] which are considered in more detail in Appendix D.

Our interest in the copper acetate dimer was initially in the bonding of the axial ligands. NMR spectroscopy is generally useful in the study of ligand substitution processes,[35-48] and we decided to investigate the NMR chemical shift and line shape of acetic acid and acetonitrile protons in the mixed solvent with and without copper acetate. This solvent system turned out to have unusual and interesting features, since under some conditions small amounts of water present will react with the acetonitrile.

The Reactions Among Acetonitrile, Acetic Acid and Water

The reaction of acetonitrile and acetic acid. A number of peculiarities have been reported in connection with the reaction between acetonitrile and acetic acid. Kremann, Zoff and Osward[49] reported in 1922, that acetic anhydride and acetamide were present after refluxing 2 Moles acetic acid with 1 Mole acetonitrile at 98°C for a few hours. These authors did not examine the reaction mixture chemically, but based their conclusion on changes in the freezing point. They also reported that heating an acetamide-acetic anhydride mixture for 30 hours at 98°C yielded the same equilibrium mixture (83% conversion to nitrile and acid). On the other hand, however, Davidson and Skorronek[50] reported that a mixture of 0.10 mole acetonitrile and 0.20 mole of acetic acid gave no test for acetic anhydride after heating for 48 hours on the steam-bath. In the same paper, however, at a

temperature of about 200°C, Davidson and Skovronek reported that various nitriles and acids reacted at elevated temperature to give not only diamides but also the corresponding anhydride and amide, due to the interlocking equilibria shown below.

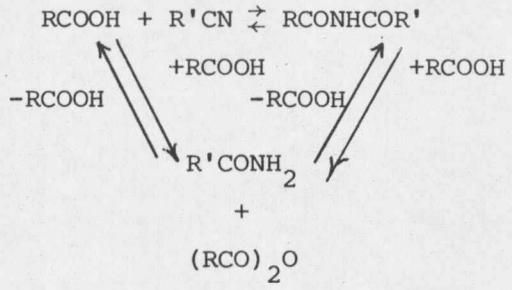

(1)

Moreover, in 1963, equilibria and relative reaction rates in the reactions of acetic and trifluoroacetic acids with acetonitrile and trifluoroacetonitrile were reported by Durrell, Young and Dresdner.[51] In contrast to the results of Davidson and Skovronek, they did not detect the presence of the anhydride-amide pair in any of their four systems. As to the pair of acetic acid-acetonitrile, their end products were still the unchanged acetonitrile and acetic acid. This discrepancy was explained by Durrell et al. as that an excess of free acid was used by Davidson and Skovronek. It can be seen from the diagram (12) that presence of excess acid would force the total equilibrium toward the amide-anhydride pair.

From the previous references and discussion, it is quite reasonable to conclude that at temperatures of lower than 50°C and

without a catalyst the net reaction of our 40%, 30%, 20% and 10% HAc/CH_3CN is

$$CH_3CN + CH_3COOH \rightleftarrows CH_3COOH + CH_3CN \qquad (2)$$

The influence of small amount of water in our acetonitrile/acetic acid solutions. The IR spectra showed the presence of water, if the HAc/CH_3CN solutions were prepared less than a week before. However, after standing for three weeks, there was no more water peak shown in the IR spectra. Apparently, the presence of HAc accelerates the hydrolysis of CH_3CN.[52] Since there is only a small amount of water in commercial acetonitrile and acetic acid, by mixing acetic acid and acetonitrile, we get only a trace of acetamide because the hydrolysis of acetonitrile.

RESEARCH OBJECTIVES

Copper acetate dimeric molecule has been an interesting topic in research. Recent literature indicates that with NMR one may study the axial ligand exchange of the dimer. We also believed that there might also be bridging ligand exchange at higher temperature, and wanted to clarify this point by NMR study of an additional mixed solvent system. We were interested in studying copper acetate in acetic acid-acetonitrile solutions to gain further insight into the bonding of axial ligand.

EXPERIMENTAL

Dimer/Monomer Equilibrium of Copper(II) Acetate in Mixture of Acetonitrile/Acetic Acid/Water from Optical Measurements

The absorbance due to both copper acetate and water were taken on Cary Model 14 spectrophotometer. Data were taken at different days for 0.005M copper acetate dimer in various percentages of acetic acid/acetonitrile solutions, and the above HAc/CH_3CN solutions containing various amounts of water.

The spectrophotometer cell was immersed in a thermostatted water bath of 24.5°C between measurements for some series of measurements. The spectrophotometer cell was equipped with a ball and socket closure and a quartz spacer allowing path lengths of 1, 3, or 10 mm. The water concentrations were calculated from the measured absorbance at 1410 nm in the near infrared using the relationship $M_{H_2O} = 3.9(a_{1410} - a_{1300})$. It was necessary to add the water concentration in the blank, determined by the same measurement vs. a cell with dilute acetic anhydride in acetonitrile.

Just before or after the near infrared scan the visible spectrum was recorded usually with a 3 mm pathlength, and $a_{690} - a_{490}$ was calculated for a 10 mm pathlength. The dimer has a substantial extinction coefficient at 690 nm ($\varepsilon_{690} - \varepsilon_{490} = 426$) and is responsible for most of the observed blue green color. The monomer absorbs in the same wavelength region, but much less strongly. The value $(\varepsilon_{690} - \varepsilon_{490}) = 35$ is taken from measurement in acetic

acid-water solutions. With these two values it is a simple matter to solve for the concentrations of both monomer and dimer.[26] The monomer concentration is negligible in the dry solutions.

Proton Magnetic Resonance Study of the Solvation of $Cu_2(OAc)_4.2H_2O$ in Acetonitrile/Acetic Acid/Water Mixtures

One set of solutions are prepared by mixing CH_3CN and HAc in given volume percentage ratios of HAc:CH_3CN = 40:60; 30:70; 20:80; 10:90. Another set of solutions were prepared by dissolving 0.005M $Cu_2(OAc)_4.2H_2O$ in previous mixed HAc and CH_3CN solutions in the same volume percentage ratios as set 1. These two sets of solutions were made up and measured. They were identical, except that one set contained 0.005 M $Cu_2(OAc)_4.2H_2O$. In order to reach the equilibrium point of the H_2O/HAc/CH_3CN solutions, samples used for measurements were more than two weeks old. The samples were stored in a desiccator. The PMR spectra were recorded with a HA-100 spectrometer equipped with a V-4341 Variable Temperature Accessory. The temperature was determined by measurement of the peak separation in methanol and ethylene glycol, and was measured and controlled to within ±2°C. Coaxial NMR tubes were used, TMS in the inner tube was used to lock on. The temperature was varied between 37.1°C and -45.2°C. The PMR line shift and line width contribution, due to hyperfine and dipolar interaction with the paramagnetic species, were measured as the

difference of the peak frequencies and widths in these two sets of solutions. Some of the measurements were repeated as many as three times. The reproducibility was quite good, but in a few cases the acid proton peak from acetic acid was at higher field than expected, by as much as 0.2 PPM. Shift even larger than this in this direction are easily produced by the addition of small amounts (about 1 microliter) of water to the sample in an NMR tube.

RESULTS

PMR Signals of Acetonitrile, Acetic Acid Methyl Protons and PMR Signals of Acetic Acid Acidic Group Proton

Chemical shift. It has been very hard to lock on TMS, since TMS in the inner tube is such a little amount comparing with the amounts of acetonitrile in the outside tube. I could lock on TMS and keep it only when the machine was in very good tune. Even though the following data are not all perfect, however, every piece of datum means that there was a happy tuning day, because more than half of my time was spent without any results. The complete data are summarized in Tables 1-11, and 14-35.

In general, the results are quite reproducible and correspond to dry solvent. For example, on November 3, 1975, I ran the 10%, 20%, 30% CH_3COOH/CH_3CN with and without .005 M $Cu_2(OAc)_4.2H_2O$ solutions twice at room temperature. That is, I had to move the inner tube around from one outside tube to another. Table 1 shows that I could get the same result for repeated measurements on the same sample. This tells us that H_2O in the air is not a serious problem even when the inner tube was changed.

When I ran my solutions on the Cary 14 in June, 1975, I observed the H_2O peak at 14100 was decreased after a couple of weeks. Also when I ran the NMR, the chemical shift of the acid proton peak of acetic acid changes from time to time. Usually, the later the date, the more downfield the position. All of these suggest that acetic

Table 1. Time: November 3, 1975; Temp: 37.0°C

Functional proton	C.S.(Hz)						L.W.(Hz)					
	10%	10% Cu	20%	20% Cu	30%	30% Cu	10%	10% Cu	20%	20% Cu	30%	30% Cu
HAc	944	936	1008	1004	1048	1049	12	12	3	4.4	2	2.2
CH_3COOH	210		210	213	213	213	2		0.8	3.5	.7	3.8
CH_3CN	205	203	205	204	208	206	2	2	1.4	1.5	1.0	1.3
After switching the inner tube around												
HAc	944	938	1009	1004	1048	1049	11	11	3.2	4.6	2.2	2.4
CH_3COOH	210		211	214	212	214	0.5		0.8	3.5	1.1	4.0
CH_3CN	207	205	207	204	206	206	1.4	1.7	1.1	1.7	1.6	1.7

C.S. = Chemical Shift; L.W. = Line width

acid in the solution catalyzes the hydrolysis of acetonitrile in the solution, and made the sample drier after long standing.

In order to have a closer understanding of the hydrolysis of CH_3CN, on October 23, 1975, I added 1 λ H_2O to some of my samples, and the results are listed in Table 2. From Table 2, we see that the addition of 1 λ H_2O causes a pronounced shift of the position of the acid proton peak of acetic acid upfield, toward TMS, about 30%. The next day the position moved back downfield again about 10%. However, after that, the chemical shifts stayed at about the same positions. Anyway, we did notice a significant hydrolysis one day after the addition of 1 λ H_2O. The chemical shift changes in the example cited are different from sample to sample, this was due to the amounts of the samples in the NMR tube being different. However, the hydrolysis results from the Cary 14 (not listed) showed that there were no pronounced hydrolysis changes even 3 days after the addition of 200 λ H_2O. A possible reason for the above confusion is as follows: When the sample was in the NMR probe, the temperature was about 37°C and it was spinning very fast. The spin made the solution in the NMR tube reach a homogeneous phase, and the temperature increased the hydrolysis rate. Therefore, the second runs after the addition of H_2O were the ones that showed that a pronounced hydrolysis reaction had occurred. After that, the hydrolysis rates became very slow again.

Table 2: Chemical Shift and Line Width of HAc before and after the addition of 1 λ H_2O

Sample	dry	10/15	10/23	10/24	10/25	10/26	dry	10/15	10/23	10/24	10/25	10/26
40%	1069		1018	1035	1035	1035	2.0		17	3.0	3.2	3.0
30%	1048		994	980	980	980	2.0		27	6.0	5.0	4.4
20%	1011		976	988	988	986	3.4		16	5.4	6.2	5.4
15%	983		897	923	925	925	5.8		35	11	12	9.8
10%	944		820	857	858	853	8.2		56	18	16	17
20% Cu	1004		903	919	919	921	4.4		19	8.6	9.0	9.0
30% Cu	1049		989	1010	1010	1010	2.2		24	4.6	5.0	4.2
40% Cu	1067	1031	1031	1034	1037	1035	2.0	6.4	6.2	3.6	4.0	4.0
	Chemical Shift (Hz)						Line Width (Hz)					

Table 3. Chemical Shifts and Line Widths of methyl peaks of CH_3CN and CH_3COOH before and after the addition of 1 λ water

		40%	40% Cu	30%	30% Cu	20%	20% Cu	15%	10%	
CH_3COOH	dry	211	213	211	211	211	215	212	209	Position (Hz)
	wet	211	213	210	212	211	215	212	211	
CH_3CN	dry	206	205	207	203	207	204	208	206	
	wet	206	206	206	204	208	206	208	208	
CH_3COOH	dry	1.3	4.1	0.8	4.0	0.8	4.0	1.0	0.6	Line Width (Hz)
	wet	0.7	4.3	0.6	5.2	0.9	5.0	0.7	0.6	
CH_3CN	dry	1.5	1.2	1.9	1.3	1.1	1.5	1.0	1.5	
	wet	0.7	1.6	0.6	0.8	0.8	1.0	0.8	0.8	

However, in the running of IR, there was no such thing as spin and also the sample was put in a thermostat of 24.5°C between the runs.

From the above discussion, we can conclude that whether a sample is a first-run or second-run sample, makes a lot of difference to the data. This can also explain the abnormal relationship between the results of October 16 and November 5 of 10% CH_3COOH/CH_3CN with and without .005 M $Cu_2(OAc)_4.2H_2O$ solutions (Tables 4-7). That is, because the samples become drier and drier, the chemical shifts of HAc usually shift more and more downfield. However, for the 10% with and without Cu samples, the chemical shifts of HAc on November 5, 1975 were smaller than those on October 16. The reason for this confusion is that the NMR samples I ran on November 5 were first-run samples while those of October 16 were not. Therefore, even though November 5 was later than October 16, still the samples were not so dry as those of October 16, and the chemical shifts were more upfield than those of October 16. However, since November 5 was quite a long time from July 7 which was the date I prepared the solutions, therefore the difference was not significant.

On August 8, 1975, we observed a more complex irreproducible behavior. The 30% HAc/CH_3CN with a Cu solution showed a shift in the acid proton peak position with temperature showing a minimum. Data observed are given here in Table 8. The explanation of this behavior is that the sample was a first-run sample, therefore it was not in a

Table 4. Time: November 5, 1975
Sample: 10% HAc/CH_3CN
Temp: Room → Low

T(°C)	HAc	
	C.S.(Hz)	L.W.(Hz)
-36	1020	40
-32	1014	32
-27	1004	26
-18	989	24
-6	980	18
+6	967	16
+17	958	13
+30	950	12
+37		

Room → Low: This means the measurement was run from room temperature to low temperature

Table 5. Time: November 5, 1975
Sample: 10% HAc/CH_3CN with .005M $Cu_2(OAc)_4 \cdot 2H_2O$
Temp: Low → Room

T(°C)	HAc	
	C.S.(Hz)	L.W.(Hz)
-32	1004	32
-27	996	32
-22	990	28
-18	983	23
-11	978	18
-6	976	18
+6	966	18
+17	954	16
+30	946	13

Table 6. Time: October 16, 1975
Sample: 10% HAc/CH_3CN with 0.005M $Cu_2(OAc)_4.2H_2O$
Temp: Room → Low

T(°C)	HAc		CH_3CN	
	C.S.(Hz)	L.W.(Hz)	C.S.(Hz)	L.W.(Hz)
-40	1030	66	207	2.8
-36	1019	69	207	2.6
-27	1006	66	207	2.2
-22	999	66	207	1.8
-18	990	66	207	1.8
-6	986	62	207	1.8
+6	979	20	207	2.3
+17	968	17	207	2.5
+30	960	12	206	1.7
+37	939	10	205	2.0

Table 7. Time: October 16, 1975
Sample: 10% HAc/CH_3CN
Temp: Low → Room

T(°C)	HAc		CH_3CN	
	C.S.(Hz)	L.W.(Hz)	C.S.(Hz)	L.W.(Hz)
-45	1070		206	3.3
-40	1059	80	206	2.2
-36	1038	74	206	2.2
-27	1025	66	206	1.6
-18	1006	60	206	2.0
-6	988	40	206	1.6
+6	976	32	205	2.0
+17	955	13	205	2.0
+30	945	12	205	1.4
+37	942	8	205	2.0

Table 8. Time: August 8, 1975
Sample: 30% HAc/CH_3CN with .005M $Cu_2(OAc)_4 \cdot 2H_2O$
Temp: Low → Room

T(°C)	HAc		CH_3COOH		CH_3CN	
	C.S.(Hz)	L.W.(Hz)	C.S.(Hz)	½ L.W.(Hz)	C.S.(Hz)	½ C.W.(Hz)
-40	1062	36	One broad peak at 207 (12 Hz)			
-36	1077	30	One broad peak at 205 (9 Hz)			
-32	1087	21	207	2.5	203	
-27	1095	17	207	2.5	203	1.7
-22	1088	14	208	2.5	203	1.8
-18	1083	9	208	2.3	203	1.7
-11	1077	8	208	2.3	203	1.6
0	1061	5	209	2.5	203	1.5
11	1048	4	210	2.6	203	1.2

Table 9. Time: November 6, 1975
Sample: 30% HAc/CH_3CN with .005M $Cu_2(OAc)_4 \cdot 2H_2O$ + 1 λ H_2O
Temp: Room → Low → Room

T(°C)	HAc	
	C.S.(Hz)	L.W.(Hz)
+37	1045	4.0
+30	1036	8.0
+17	1043	12.0
+6	1045	16.0
-6	1054	10.0
-18	1066	9.0
-27	1079	14.4
-32	1085	16.0
-35	1090	15.0
-36	1093	18.0
+37	1027	4.0

homogeneous phase, and it was pretty wet too. Due to a change with time in the H_2O concentration in the part of the solution in the region sampled by the spectrometer, thus the first two results were not consistent. Since the sample was run from low temperature to room temperature, therefore the chemical shifts of -40°C and -36°C were not consistent. This reason can be supported by the experiment I ran on November 6, 1975. From Table 9, we can see clearly that the chemical shift of the first measurement, room temperature, was wrong, for the same reason as given above. Apparently, the NMR solution was not homogeneous in the first run.

Table 11 is the data of positions of acid proton peak on dry solutions of 100% HAc, 40%, 30%, 20%, 15%, 10% and 5% HAc/CH_3CN without .005M $Cu_2(OAc)_4.2H_2O$, and their CH_3CN Moles/HAc Moles ratios: From Table 10, we can conclude that the effect of copper acetate on the position of the acid peak of acetic acid is small. We can fit the positions of the acid peak of acetic acid in the HAc-CH_3CN mixtures by an appropriate temperature dependent dimerization equilibrium. The following is the detail of the calculation:

Acetonitrile: density, 0.7856g; Molecule weight, 41.05

Acetic Acid: density, 1.0491g; Molecule weight, 60.05

X_o = Wt. HAc/ MW HAc; Y_o = Wt. CH_3/MW CH_3CN

Y_o/X_o = CH_3CN Moles/HAc Moles $X_{HAc} = X_o/(X_o + Y_o)$

Table 10. Chemical Shift (Hz) of Acidic proton of HAc

T(°C)	10%	10% Cu	20%	20% Cu	30%	30% Cu	40%	40% Cu
-45						1130		
-40						1124	1152	1146
-36	1020				1125	1112	1145	1137
-32	1014	1004					1141	1134
-27	1004	996	1072	1068	1112	1111	1135	1126
-22		990					1127	
-18	989	983	1058	1055	1103	1102	1121	1122
-11		978	1054				1116	
-6	980	976	1046	1043	1090	1090	1112	1113
0							1108	
+6	967	966	1040	1030	1080	1081	1104	1103
+11							1100	
+17	958	954	1025	1018	1069	1068		1094
+30	950	946	1015	1008	1059	1061		1084
+37	944	938	1009	1004	1048	1049	1069	1067

Table 11. Chemical shifts of acid proton peak of HAc of 5, 10, 15, 20, 30, 40, 100% HA/CH_3CN solutions, and their CH_3CN Moles/HAc Moles ratios

Solution	5%	10%	15%	20%	30%	40%	100%
HAc C.S.*(Hz)	858	944	983	1010	1048	1067	1174
$\frac{CH_3CN\ Moles}{HAc\ Moles}$	20.81	9.86	6.21	4.38	2.16	1.64	0

*C.S. = Chemical Shift; L.W. = Line width

The Y_o/X_o values for 5, 10, 15, 20, 30, 40, HCN/CH_3CN solutions are 20.813, 9.8591, 6.2074, 4.3817, 2.1636, 1.6430 and 0, respectively.

$$2HOAc \rightleftarrows H_2O_2Ac_2$$

$$X \qquad (X_o-X)/2$$

Total Moles: $Y_o + X + (X_o-X)/2 = Y_o + X_o/2 + X/2$

$$K = \frac{(HAc)^2}{(Dimer)(Total)} = \frac{X^2}{(\frac{X_o-X}{2})(Y_o+\frac{X}{2}+\frac{X_o}{2})} + \frac{2(\frac{X}{X_o})^2}{(1-\frac{X}{X_o})(\frac{Y_o}{X_o}+\frac{1}{2}+\frac{X}{2X_o})}$$

$$\text{let } z = \frac{X}{X_o}, \quad K = \frac{2z^2}{(1-z)(\frac{1}{2}+\frac{Y_o}{X_o}+\frac{X}{2X_o})}$$

$$(4 + K)z^2 + K(2Y)z - K(1 + 2y) = 0$$

Assume K, calculate X/X_o for 7 values of Y_o/X_o

and the results from computer calculation are as follows:

$$K = .175 \pm .050$$

$$\text{Position for Dimer} = 1286 \pm 26 \text{ (cps)}$$

$$\text{Position for Monomer} = 705 \pm 20 \text{ (cps)}$$

Then from the position of dimer and monomer, we can get

$$\text{Monomer fraction} = (1286-\text{Chemical Shift})/(1286-705) = F$$

$$\text{Moles of Dimer} = (1-\text{Monomer fraction})/2 = D$$

$$K = (\text{Monomer fraction})^2/(\text{Dimer fraction})(Y_o/X_o + F + D)$$

Tables 12 and 13 are the lists of calculated HAc monomer fractions and the equilbrium constant K. Putting the equilibrium constants (K) and chemical shift (Table 10) of different temperatures and compositions into a computer program, we got F(1) = -1.73083, F(2) = -897.059deg^{-1} for the reference temperature 37°C. From the data we got from the computer, we plot lnK vs 1/T

Intercept = F(1) = lnK at T = 310°K

Slope = $-\Delta H/R$ = F(2)

ΔH = slope . R = (-897.059) x (1.98717) = 1782.7 cal/Mole

$K = e^{-\Delta H/RT} e^{\Delta S/R}$

$$\ln K = -\frac{\Delta H}{R}\left(\frac{1}{T}\right) + \frac{\Delta S}{R}$$

Table 12. HAc monomer fractions of different solutions at different temperatures

T(°C)	$\frac{1000}{T}$	HAc monomer fraction 10%	20%	30%	40%
-40	4.3				.2306
-36	4.22			.275	.2427
-32	4.15	.46816			.2496
-27	4.07	.48537	.368	.2993	.2599
-22	3.98				.2737
-18	3.92	.5112	.3924	.3150	
-11	3.82		.3993		.2926
-6	3.745	.5267	.4131	.3374	.3012
0	3.66				.3064
6	3.58	.549	.4234	.3494	.3133
11	3.52				.3204
17	3.45	.5645	.4492	.3735	
23					
30	3.30	.5783	.446	.3838	
37	3.226	.5886	.4768	.4096	.3770

Table 13. Dimer-Monomer equilibrium constant of different solutions at different temperatures

T(°C)	K			
	10%	20%	30%	40%
-40				.06012
-36			.042	.06869
-32	.07781			.0732
-27	.08636	.0846	.0908	.0803
-22				.0905
-18	.10072	.0998	.1027	.100
-11		.10448		.10573
-6	.11034	.11427	.1213	.11321
0				.1179
6	.12473	.1221	.132	.1243
11				.1476
17	.13756	.1435	.1562	
23				
30	.1518	.1594	.1675	
37	.1581	.1697	.198	.196

Our Reference Temperature T = 310°C

$-1.73083\ R = -2100/310 + \Delta S$

$\Delta S = 3.35$ Cal/Mole Deg

The following figure is the plot of lnK vs. 1000/T

Line width. Generally, the results of all the line width measurements are quite consistent. For the line widths of HAc acidic proton, from Table 14, we can observe that in no case is there much change in the width of the peak on adding copper acetate, however, the data do show a small consistent increase in width on adding copper acetate, especially for 10% and 20% solutions. The line width is larger in the order of 10% > 20% > 30% > 40%, and the line width increases with decreasing temperature. Addition of 1 λ water to the solutions broadens the line width of the HAc acid proton. Table 2 is the line widths of HAc before and after the addition of 1 λ water. The line width changes in the example cited are different from sample to sample, the main reason was due to the amounts of the sample in the NMR tube being different. The peak shift and broadening on the addition of water are clearly due to hydrogen exchange between water and acetic acid. This was not considered important enough to pursue further, particularly since water reacts with the acetonitrile, thus the data is limited to single addition of water at room temperature.

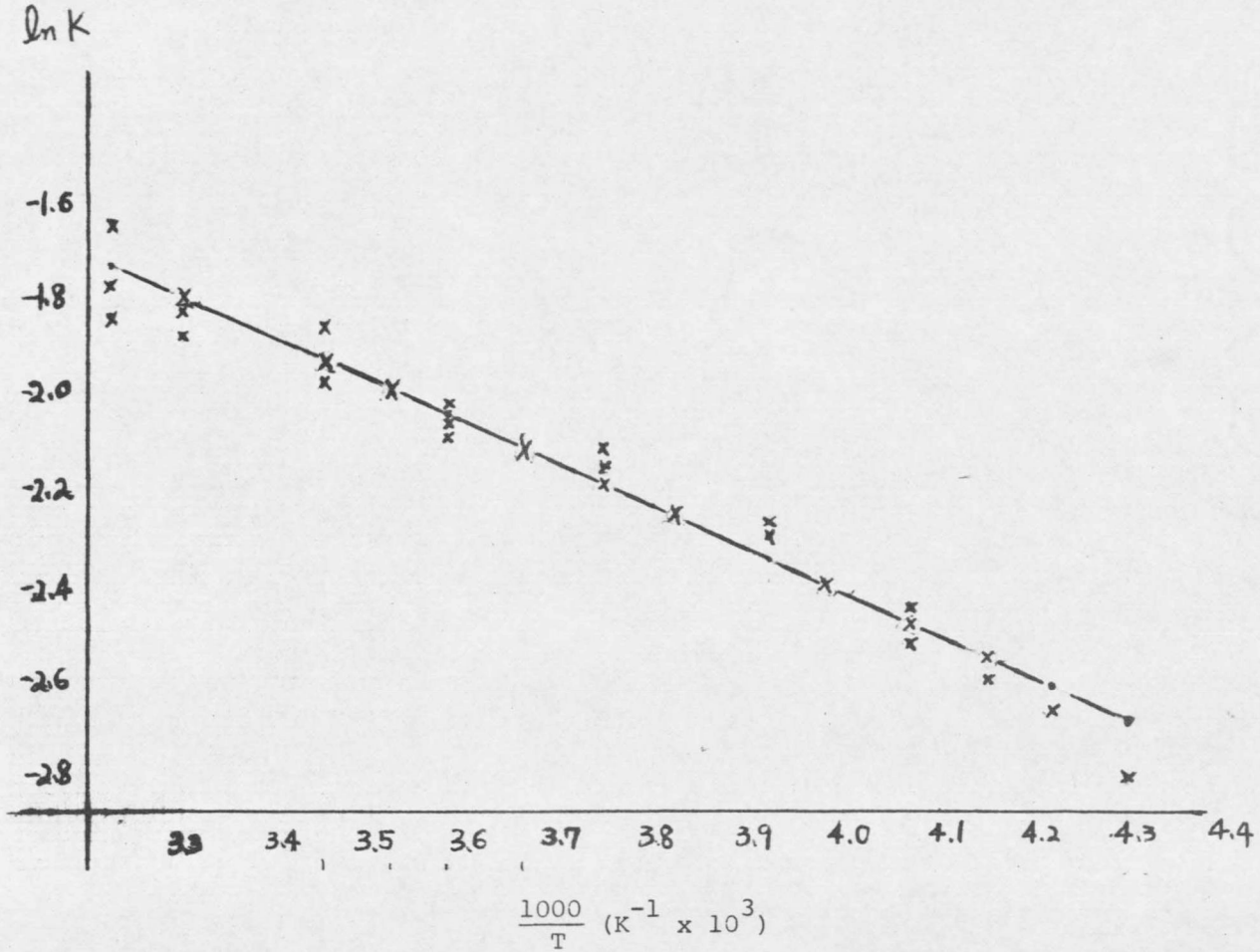

Figure 2. Plot of lnk vs. 1000/T
Points (x) represent measured values. The straight line is calculated.

Table 14. Line Width (Hz) of Acidic proton of HAc

T(°C)	10%	10% Cu	20%	20% Cu	30%	30% Cu	40%	40% Cu
-45			26	36		24		
-40			22	28	15	15	10.4	
-36	34		16		11	12.4	8.6	9.4
-32	32	32		24			7.4	8.4
-27	26	32	12	16	6.4	8.2	6.6	8.0
-22		28					5.8	
-18	24	22	10	14	4.4	7.0	4.8	6.0
-11		18					4.2	
-6	18	18	9.2	9.6	3.2	5.6	4.4	5.4
0							4.0	
+6	16	18	5.8	7.2	2.6	5.0	3.6	4.8
+11							2.4	
+17	13	16	4.4	6.2	2.6	4.2		4.2
+30	12	13		6.0	2.0	4.0		
+37	8	10	3.4	4.4	2.0	2.2	1.8	2.

When the temperature was not too low, we can see very clearly that addition of copper acetate broadened the line width of the methyl peak of HAc profoundly. The reason that we could not see the influence so clearly at low temperature was partly due to the fact that the peaks were already pretty broad, but the major effect is apparently a substantial activation energy for exchange with the bridging acetate groups. There is a noticeable broadening of the line width of the methyl peak of CH_3CN on either decreasing the temperature or adding the copper acetate, however, both effects are small. The addition of 1 λ H_2O had no influence on the line width of either methyl peak at all (Table 3).

The following are the individual discussions of the line widths of the methyl peak of HAc.

10% No Cu: The methyl peak is a well resolved small peak at room temperature, however, as temperature is lowered the peak becomes broader and less well resolved from the large CH_3CN peak.

10% with Cu: The broadening due to 0.005M $Cu_2(OAc)_4 \cdot 2H_2O$ is sufficient that it is a barely distinguishable shoulder from -45°C to 25°C, at 37.7°C the methyl peak with Cu present is not seen even with the best tuning. This is consistent with a rapidly increasing effect of Cu as the temperature increased above 25°C.

20% No Cu: A separate methyl group is distinguishable over the whole temperature from -45°C to 37°C. The position at 210 cps is essentially independent of temperature and the observed widths are more a function of tuning than of temperature.

20% with Cu: Spectra are practically constant from -45°C to -6°C, as temperature is raised further there is more downfield shift and increased broadening. Below is a table of its line width and chemical shift at different temperatures.

Table 15. 20% HAc/CH_3CN with 0.005M $Cu_2(OAc)_4 \cdot 2H_2O$

T(°C)	C.S.(Hz)	½L.W.(Hz)	frequency shift (Hz)
37	215	5	5
30	215	3	5
17	212	4	2
6	212	3.5	2
-6	212	2.0	2
-18	211	2.0	1
-22	211	2.5	2
-27	211	2.3	2
-32	211	2.5	2
-36	211	2.5	1
-45	210	2.5	0

30% No Cu: Peak positions are at 209 cps and all of them are well resolved at all temperatures, and just somewhat broader and slightly overlapping at -40°C.

30% with Cu: Line widths are about constant from -45°C to 0°C, as temperature is raised further, there is a little downfield shift and a little broadening. However, the concentration of HAc is quite high, therefore, the influence of copper acetate is not so clear as 20% with Cu. Its chemical shifts and line widths at different temperatures are cited below with the 40% with Cu.

40% No Cu: Peak positions at 209 cps, well resolved at all temperature, just somewhat broader and slightly overlapping at -40°C. The peak is broadened as a function of temperature.

40% with Cu: Since the concentration of HAc is so high that the influence of copper acetate on line width was not noticeable even at room temperature. However, we can see the influence of copper acetate on chemical shift at 30°C. Following is a table of its line width and chemical shift at different temperatures.

From the above discussion, we would like to summarize line width in the following three respects:

Table 16. The Line Width, Chemical Shift and frequency shift of methyl peak of 30 and 40% HAc/CH_3CN with .005M $Cu_2(OAc)_4.2H_2O$

T(°C)	½ L.W.(Hz)		C.S.(Hz)		frequency shift (Hz)	
	30% Cu	40% Cu	30% Cu	40% Cu	30% Cu	40% Cu
-45	4.0		207		0	
-40		4.0		208		0
-36	4.1	4.0	207	208	0	0
-32	4.0	4.0	207	208	0	0
-27	4.0	4.0	208	208	0	0
-22	4.0		208		0	
-18	4.0	3.8	208	209	0	0
-11	4.0		208		0	
0	5.0	4.0	209	209	0	
6						0
11	6.0	4.0	209	211	0	0
17		3.8		211		1
30		4.0		213		2
37	6.0	4.0	210	213	2	3

1) For acidic proton of HAc, rate of acid proton exchange between acetic acid monomers and dimers is fast even down to -30°C, a low activation energy is expected for a plot of line width (sec^{-1}) vs. 1000/T. We can estimate τ_M from the total transverse relaxation rate $1/T_2$. $1/T_2$ is calculated from the experimental PMR line width, using the relaxation $1/T_2 = \delta\omega/2$ which applies for a Lorentzian line shape, when $\delta\omega/2\pi$ is the full line width of Hz at half maximum.

2) The exchange of acetic acid and acetonitrile into the axial position of the copper acetate dimer is fast even at low temperature. There is a small effect of $Cu_2(OAc)_4$ on the acid peak of acetic acid and the methyl group of CH_3CN. Since the effect is small, quantitative treatment is not possible. It is clear that this exchange is fast even down to -30°C. A low activation energy is expected. Since bonding of axial ligands is very weak, we expect just such behavior, i.e., small effect and fast exchange even at low temperature.

3) The rate of exchange of acetate between acetic acid and the bridging positions in $Cu_2(OAc)_4$ is slower. This produces a large effect at the highest temperatures on both peak position and line width, but only for the methyl group protons of the acetate, the only protons still present in the bridging ligand.

Finally, we would like to explain our phenomena by the assumption of the existence of axial ligand exchange, bridging ligand exchange, and the acid proton exchange between acetic acid monomer and dimer.

1) At the axial position, there is ligands exchange of both HAc and CH_3CN. Both HAc and CH_3CN must be present as axial ligand to explain why the extinction coefficient at 690 nm for the copper acetate dimer is 426 instead of 370 which is the extinction coefficient at 690 nm if the acetic acid is the only ligand on the axial position. The extinction coefficient is 466 for a 100% CH_3CN solution.

2) Since the distance of the axial ligand to Cu is quite far and bonding of axial ligand is very weak, therefore there is smaller effect by the Cu and low activation energy for the ligand exchange. The former reason explains why there is only a little broadening of methyl peak of CH_3CN by the addition of Cu, the latter reason explains why the CH_3CN axial exchange is fast even at low temperature.

3) For the acidic proton of HAc, there are two factors which influence the chemical shift and line width. There are the axial ligand exchange of copper acetate and the acid proton exchange between acetic acid monomer and dimer. There is only a little chemical shift change by the addition of Cu which is a function of $C_{HAc}/C_{Cu_2Ac_4}$ ratio, however there is a pronounced chemical shift change for

different concentration of HAc. This means the dimer-monomer exchange has stronger influence than the axial ligand exchange and will be considered first. The following is the explanation of different chemical shift and line width based on the above assumption: (a) Chemical shift in the absence of Cu: Since the fraction of dimer is increasing in the order of 10 < 20 < 30 < 40%, therefore the chemical shift (Hz) is increasing in the same order; (b) Line width in the absence of Cu: The more dimer fraction there is, the faster the dimer-monomer exchange is, therefore the sharper the peak is; (c) Effect of Cu: The small shift and broadening by the addition of Cu is due to the presence of axial ligand exchange. These observations are qualitatively similar to the effect of Cu on the acetonitrile peak and on the methyl peak of acetic acid at temperatures below -10°C. As the C_{HAc}/C_{CuAc_2} ratio increased, the influence of Cu is decreased.

4) For the methyl protons of HAc with Cu. At lower temperature, because the presence of axial exchange, there is a little broadening by the addition of Cu. Because the activation energy of the axial ligand exchange is low, the line width for the methyl protons stays almost the same from -6°C to -40°C. However, at 37.1°C, since there is enough energy for the bridging ligand exchange to occur at an appreciable rate, a significant broadening and downfield shift was noticed at room temperature.

Using the above assumptions, we can also explain the results of recently PRM study of the solvation of copper acetate dimeric molecules in ethanol/acetic acid mixture by Grasdalen.[53] With their NMR equipment, they have measured NMR line width and line shift of the solvent protons in ethanol/acetic acid solutions of copper acetate between -100°C and 100°C. Although they could not measure the acidic protons of acetic acid because it exchanged rapidly with the alcoholic hydrogen of ethanol, they got a very wide range of measurements for the methyl proton of CH_3COOH. The following two figures (3 and 4) are their results.

From the above-mentioned two figures, we can see that their results of the chemical shifts and line width of the methyl proton of HAc are consistent with ours and can be very well explained by the discussion we made before. However, completely forgetting about bridging ligand exchange, they attempted to interpret the above results on the assumption of a selective solvation of acetic acid on the axial positions of the copper acetate dimeric molecules. In order to explain the broadening and downfield chemical shift at higher temperature as shown in Figures 3 and 4, they suggested a structure of a copper acetate dimeric molecule with one axial ligand and one second coordinated HAc ligand as shown in Figure 5. However, their suggestion is in conflict with many facts and we would like to discuss these as follows:

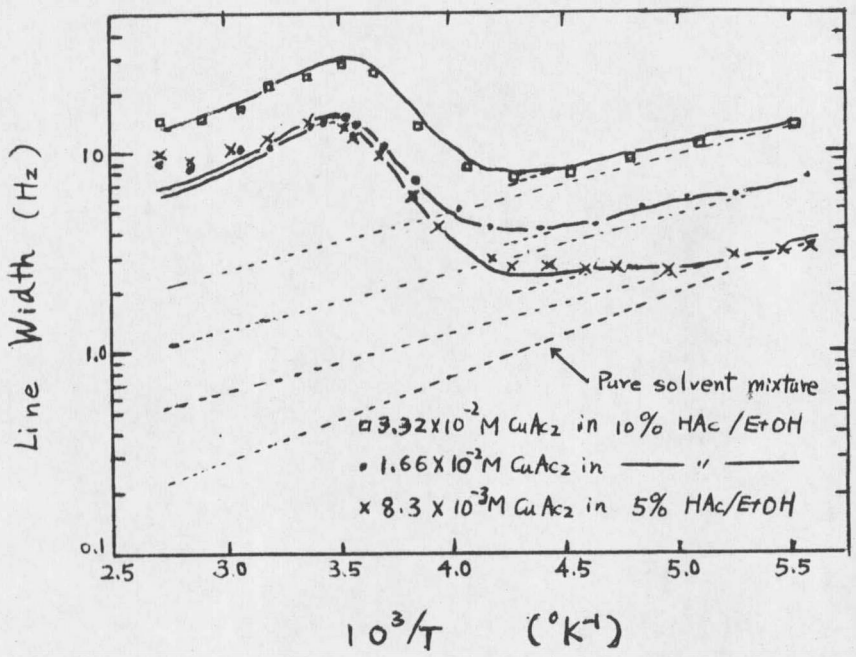

Figure 3. NMR line width of HAc methyl protons in ethanol/acetic acid solutions of $CuAc_2$ as a function of the reciprocal temperature, copper acetate concentration, and the $HAc/CuAc_2$ ratio. Points represent measured values where the solvent contribution (the dash-dot line) has been subtracted. The curves are calculated as explained in the text.

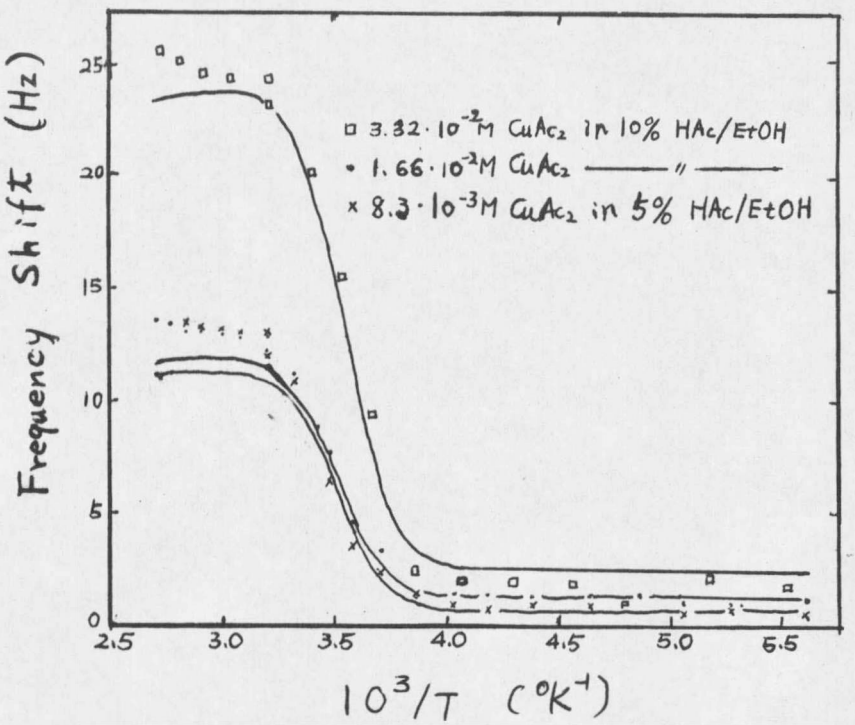

Figure 4. NMR line shift of HAc methyl protons in ethanol/acetic acid solutions of $CuAc_2$ as a function of the reciprocal temperature, copper acetate concentration, and the $HAc/CuAc_2$ ratio. Points represent measured values. The curves are calculated.

1) Their axial ligand exchange activation energy $\Delta H = 10.7$ Kcal/Mole is too high for axial ligand exchange.

2) In order to explain Figure 4, they said that at low temperature, the exchange between solvated and bulk acetic acis is too slow to shift the observed bulk peak. However, this is proved wrong by our downfield chemical shift and broadening of acidic proton peak of HAc which proved the exchange of the axial ligand is fast even at that low temperature.

3) For Figure 3, in order to explain the line width broadening of methyl peak of HAc at higher temperature, they suggested that the second coordinated HAc molecule is hydrogen bonded to the carboxy oxygen opposite to the hydrogen bond formed by the axial ligand; if this did happen, then we should get a broadened acidic proton peak of HAc with Cu at the corresponding temperatures too, however, the acidic peak is sharper with increasing temperature. The particular structure in Figure 5 was proposed to explain how the acid proton could be held in a particular location where the Cu atoms would not have much effect. However, the structure proposed would not be sufficiently rigid to insure this. The proper explanation of the fact that copper acetate has much more influence on the methyl hydrogens than on the acid hydrogen is that the acid hydrogen is not present when acetate exchanges into the bridging position.

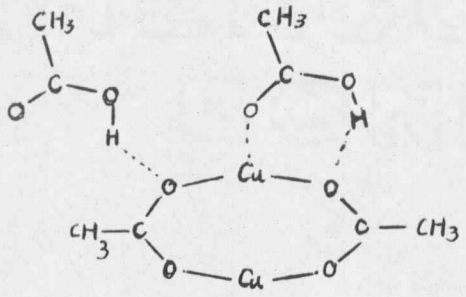

Figure 5. Grasdalen's assumed structure of a copper acetate dimeric molecule (only two bridges shown) with one axial HAc ligand and one second coordinated HAc ligand

High temperature NMR study. According to our bridging ligand exchange assumption, at 37.1°C the methyl peak of CH_3COOH is broadened because of the starting of the bridging ligand exchange. Then as the temperature is increased further, the bridging ligand exchange should be faster and the methyl peak of CH_3COOH should become sharper accordingly. It was decided to test this experimentally, and preliminary results were obtained as follows.

Because of the NMR HA100 machine not having been well tuned since November 8, therefore, in order to lock on TMS, I put TMS in both inside and outside tube, and the solution was dried before it was run. The following tables and figures are our results. From these results and by the comparison with the other NMR data, it is very clear that the methyl peak of CH_3COOH is sharper with increasing temperature above 42°C because the bridging ligand exchange is faster.

Table 17. Time: November 20, 1975
Sample: 20% and 30% HAc/CH_3CN with 0.005M $Cu_2(OAc)_4.2H_2O$
Temp: Room → High for 30% Cu; High → Low for 20% Cu

T(°C)	HAc		CH_3COOH		CH_3CN		
	C.S.(Hz)	L.W.(Hz)	C.S.(Hz)	L.W.(Hz)	C.S.(Hz)	L.W.(Hz)	
+37	1004	6	215	7.5	204	3.7	20% Cu
+42	992	6	215.5	6.5	204	4.0	
+47	990	6	215	5.0	204	2.7	
+52	979	5	217.5	4.5	204	2.5	
+58	973	5	217	4.2	205	2.5	
+37	1052	2.0	214	5	204	1	30% Cu
+45	1000	4.8	214	7	204	2	
+47	992	4.0	214	7	204	3	
+52	983	4.0	214	6	204	3.2	
+58	971	4.0	214	6	205	3.2	

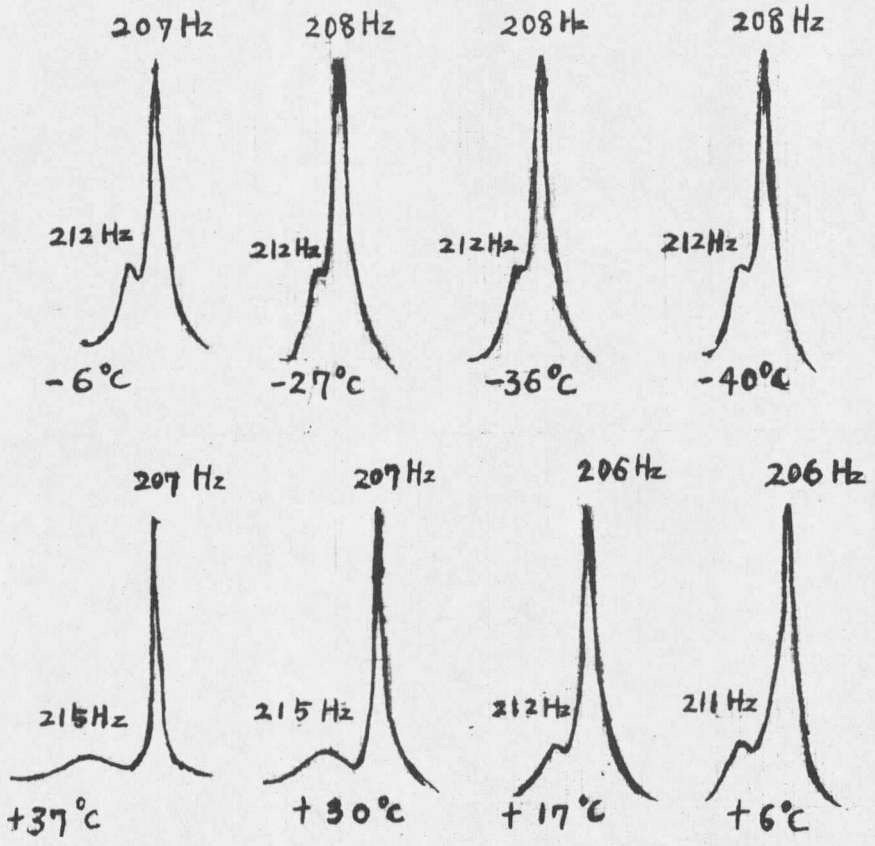

Figure 6. CH_3COOH and CH_3CN methyl lines of 20% CH_3COOH/CH_3CN with 0.005M $Cu_2(OAc)_4 \cdot 2H_2O$ from -40°C to +37°C

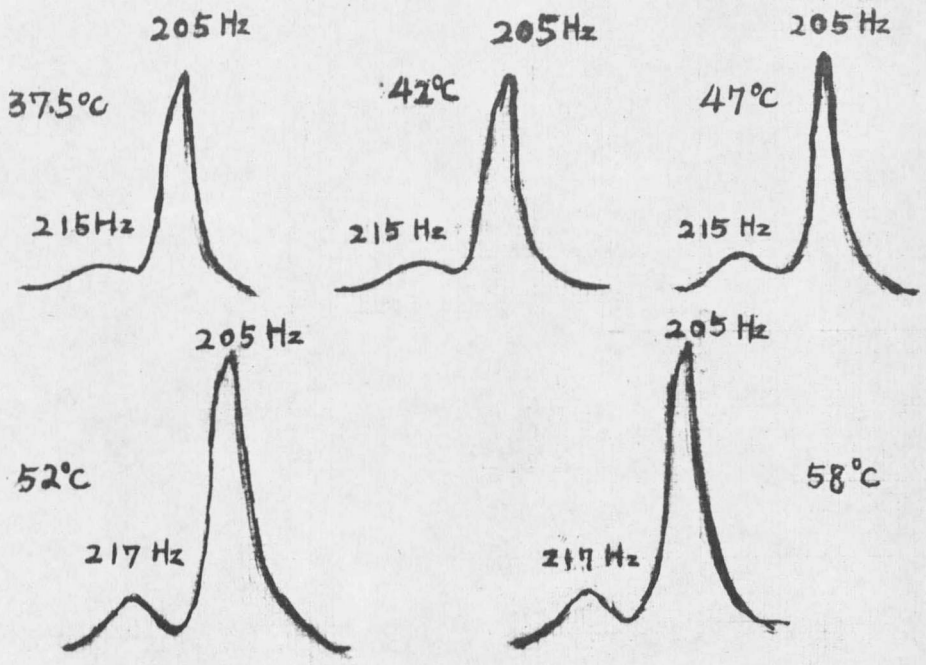

Figure 7. HAc and CH_3CN methyl lines of 20% HAc/CH_3CN with 0.005M $Cu_2(OAc)_4.2H_2O$ from +37.5°C to +58°C

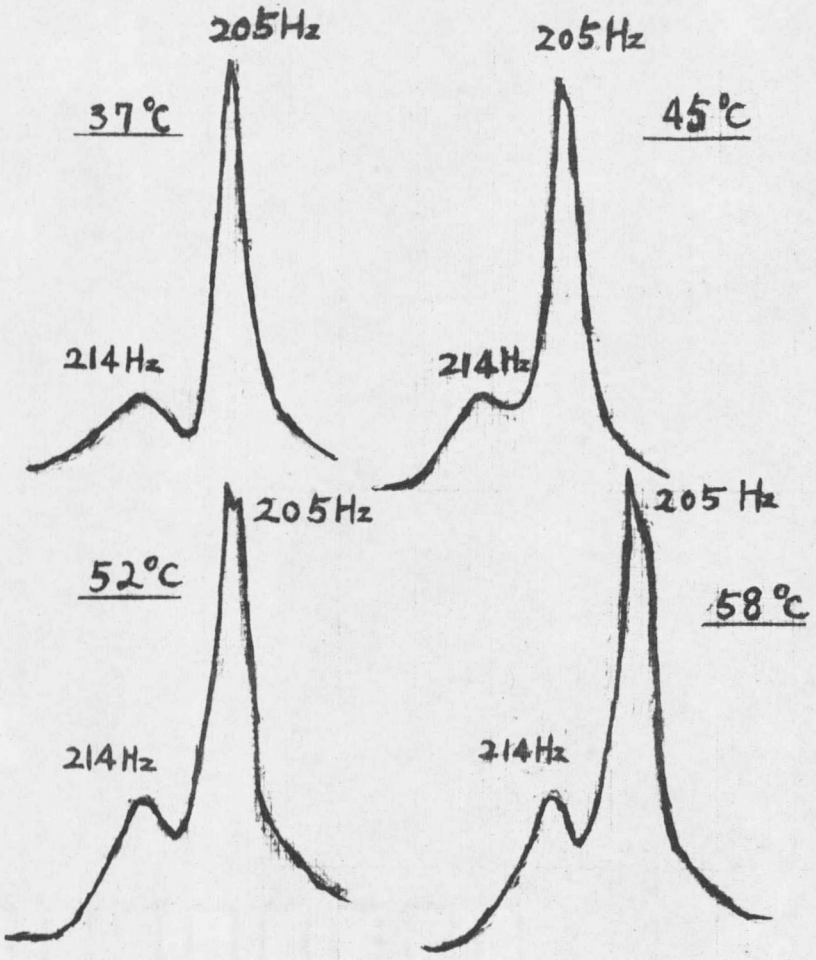

Figure 8. HAc and CH_3 methyl lines of 30% HAc/CH_3CN with 0.005M $Cu_2(OAc)_4.2H_2O$ from +37°C to +58°C

SUMMARY

The uv-visible spectra of copper acetate solutions in acetic acid - acetonitrile solutions show that both acetic acid and acetonitrile coordinate in the axial positions of the copper acetate dimer. Exchange into these axial positions introduces small changes in the PMR spectra for all the protons in both acetic acid and acetonitrile over the entire temperature range from -40 to 37°C. In addition there is a very pronounced broadening of the methyl proton peak of acetic acid on the addition of copper acetate at temperatures above -6°C. The data in this thesis establish that this effect is due to exchange of acetate between acetic acid and the bridging acetate groups of the copper acetate dimer, contrary to the interpretation proposed by Grasdalen[53] for the similar effect observed in acetic acid - ethanol mixtures.

APPENDIX A

PMR SPECTRA

While the main features of the spectra are evident from tables of the positions and widths, there are experimental complications in using the HA 100 NMR spectrometer involving variations in tuning, saturation, and spinning side bands so that more complete spectra would be valuable to someone attempting to duplicate the work. Therefore, some representative spectra and portions of spectra are reproduced here.

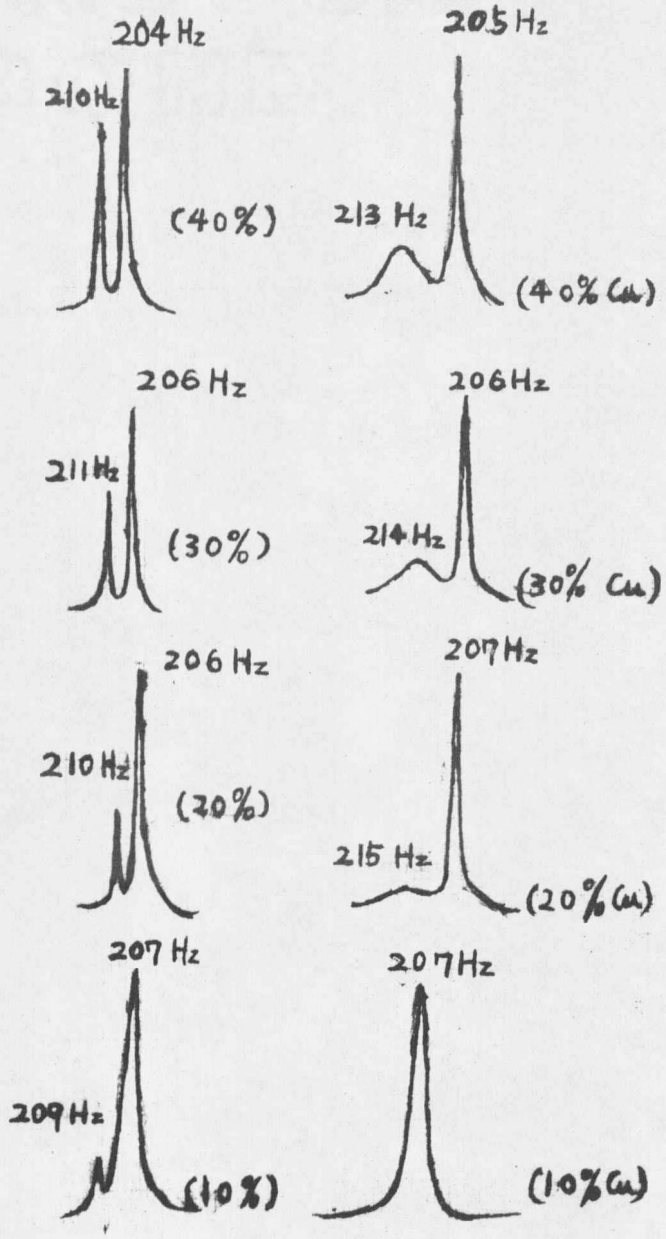

Figure 9. CH_3CN and HAc methyl lines of 10, 20, 30 and 40% HAc/CH_3CN solutions with and without 0.005M $Cu_2(OAc)_4 \cdot 2H_2O$ at +37°C

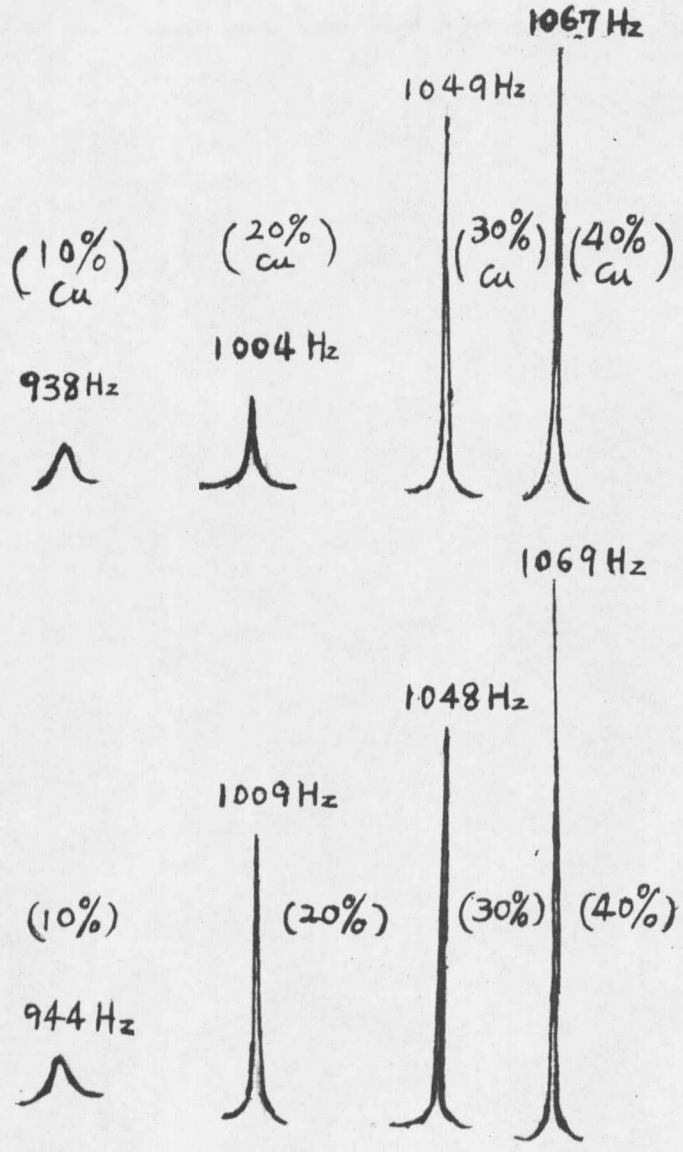

Figure 10. HAc acidic proton lines of 10%, 20%, 30% and 40% CH_3COOH/CH_3CN solutions with and without 0.005M $Cu_2(OAc)_4.2H_2O$ at +37°C

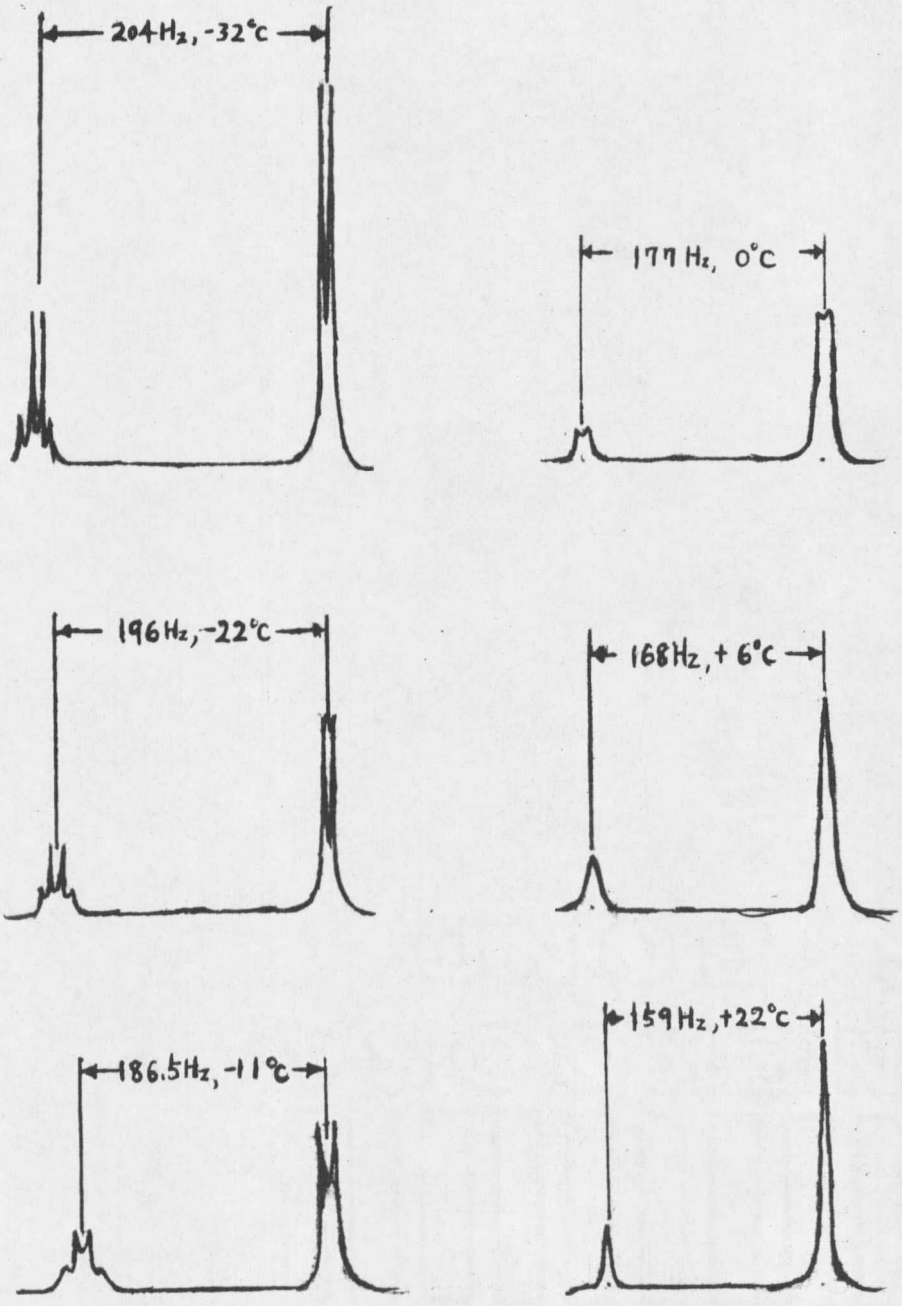

Figure 11. Representative methanol peaks which we have used to decide the relationship between regulatory settings and temperatures

APPENDIX B

PMR TABLES

Table 18. Time: October 15, 1975; Sample: 40% HAc/CH_3CN; Temperature Running Order: 37 → 30 → -36 → -32 → -27 → -18 → -6 → 6 → 17 → 30 → 37°C

T(°C)	HAc		CH_3COOH		CH_3CN	
	Position (Hz)	Line Width (Hz)	Position (Hz)	Line Width (Hz)	Position (Hz)	Line Width (Hz)
+37	1069	2.0	213	4.1	205	1.3
+30	1077	4.2	212	4.2	205	1.9
-36	1137	9.4	210	4.0	205	3.3
-32	1134	8.4	210	4.0	204	3.0
-27	1126	8.0	210	3.9	205	2.8
-18	1122	6.0	209	3.8	205	2.0
-6	1113	5.4	210	3.7	205	2.1
+6	1103	4.8	211	4.2	205	2.0
+17	1094	4.2	211	4.1	206	1.5
+30	1084	4.6	212	5.0	205	1.3
+37	1070	2.2	213	4.1	205	0.5
After the addition of 1λ H_2O						
+37	1031	6.4	213	4.7	206	1.6

Table 19. Time: August 15, 1975; Sample: 40% HAc/CH_3CH; Temp: Room → Low

T(°C)	HAc		CH_3COOH		CH_3CN	
	C.S.(Hz)	L.W.(Hz)	C.S.(Hz)	L.W.(Hz)	C.S.(Hz)	L.W.(Hz)
-47	Frozen					
-40	1152	10.4	209	4.8	204	3.0
-36	1146	8.6	209	4.5	205	3.0
-32	1141	7.4	209	4.0	205	2.5
-27	1135	7.0	209	3.9	205	3.0
-22	1127	5.8	209	2.6	205	2.6
-18	1120	4.8	209	2.5	204	2.5
-11	1116	4.2	209	2.5	204	2.6
-6	1111	4.4	209	3.0	204	2.9
0	1108	4.0	209	2.6	205	2.6
+6	1104	3.6	209	2.0	204	2.2
+11	1100	2.4	209	1.9	204	1.5
+37	1065	2.0	210	1.6	205	1.5

Table 20. Time: August 14, 1975; Sample: 40% HAc/CH_3CN with 0.005 M $Cu_2(OAc).2H_2O$; Temp: Room → Low

T(°C)	HAc		CH_3COOH		CH_3CN	
	C.S.(Hz)	L.W.(Hz)	C.S.(Hz)	½L.W.(Hz)	C.S.(Hz)	½L.W.(Hz)
-45	1101	32	208	4.6	204	2.5
-40	1095	30	208	4.0	204	1.7
-36	1089	25	208	4.0	204	1.7
-32	1083	24	208	2.7	204	1.5
-27	1076	18	208	2.7	204	1.5
-22	1071	17	208	3.0	204	1.5
-18	1068	14	209	2.7	204	1.5
-11	1062	10	209	2.5	204	1.5
0	1054	9	209	2.5	204	1.4
+6	1051	9.4	209	2.5	203	1.5
+11	1047	8	210	2.5	203	1.3
+17	1041	6	210	2.5	203	1.1

Table 21. Time: October 28, 1975; Sample: 30% HAc/CH_3CN
Temp: Room → Low

T(^{o}C)	HAc	
	C.S.(Hz)	L.W.(Hz)
-36	1122	11
-27	1110	6.4
-18	1097	4.4
-6	1083	3.2
+6	1071	2.6
+17	1061	2.6
+30	1050	2.0
+37	1046	2.0

Table 22. Time: August 8, 1975; Sample: 30% HAc/CH_3CN; Temp: Room → Low

T(°C)	HAc		CH_3COOH		CH_3CN	
	C.S.(Hz)	L.W.(Hz)	C.S.(Hz)	L.W.(Hz)	C.S.(Hz)	L.W.(Hz)
-40	1113	21	209	2.2	205	2.2
-36	1106	17	209	2.0	205	2.2
-32	1100	13	209	1.9	205	1.9
-27	1094	12	209	1.5	205	2.0
-22	1090	11	209	1.4	205	2.0
-18	1081	10	209	1.3	205	2.1
-11	1076	8	209	1.1	205	1.9
0	1066	7	209	1.8	205	1.9
+37	1027	2	210	1.6	206	1.1

Table 23. Time: October 22, 1975
Sample: 30% HAc/CH_3CN with .005 $Cu_2(Ac)_4 \cdot 2H_2O$
Temp: Room → Low

T(°C)	HAc	
	C.S. (Hz)	L.W. (Hz)
-45	1130	24
-40	1124	15
-36	1122	12
-27	1111	8
-18	1102	7
-6	1090	5.6
+6	1081	4
+17	1068	4
+30	1061	2.8
+37	1045	

Table 24. Time: October 30, 1975
Sample: 30% HAc/CH_3CN
Temp: Room → Low

T(°C)	HAc	
	C.S. (Hz)	L.W. (Hz)
-36	1126	11
-27	1112	6.
-18	1100	5.6
-6	1088	3.4
+6	1078	3.6
+17	1066	2.6
+30	1057	2.0
+37	1048	2.0

Table 25. Time: November 5, 1975
Sample: 20% HAc/CH_3CN
Temp: Low → Room

T(°C)	HAc	
	C.S.(Hz)	L.S.(Hz)
-27	1072	26
-18	1058	24
-11	1054	16
-6	1046	12
+6	1040	10
+17	1025	9.2
+23	1021	6.0
+30	1015	4.4
+37	1009	3.4

Table 26. Time: October 9, 1975
Sample: 20% HAc/CH_3CN
Temp: Room → Low

T(°C)	HAc		CH_3COOH	CH_3CN
	C.S.(Hz)	L.W.(Hz)	C.S.(Hz)	C.S.(Hz)
-45	1112	27	210	205
-40	1102	36	210	205
-36	1092	16	210	205
-27	1085	13	210	205
-18	1069	10.6	210	206
-6	1064	10.4	210	206
+6	1052	6.6	210	206
+17	1043	5.4	208	206
+37	1017	4.4		

Table 27. Time: October 9, 1975; Sample: 20% HAc/CH_3CN with 0.005M $Cu_2(OAc)_4.2H_2O$; Temp: Room → Low

T(°C)	HAc		CH_3COOH		CH_3CN
	C.S.(Hz)	L.W.(Hz)	C.S.(Hz)	½L.W.(Hz)	C.S.
-45	1049	57	212	2.5	207
-40	1043	45	212	2.5	208
-36	1035	37	212	2.3	208
-32	1027	32	212	2.3	208
-27	1024	26	212	2.5	208
-18	1013	21	212	2.0	206.5
-6	1001	18	212	3.5	207
+6	994	16	212	4.0	206
+17	975	12	212	3.0	206
+30	961	10	215	3.0	207
+37	956	6	215	5.0	270

Table 28. Time: October 30, and November 5, 1975
Sample: 20% HAc/CH_3CN with 0.005M $Cu_2(OAc)_4 \cdot 2H_2O$
Temp: Low → Room on October 30; From Room → Low on November 5

T(°C)	HAc		HAc	
	C.S.(Hz)	L.W.(Hz)	C.S.(Hz)	L.W.(Hz)
-27	1037	13	1068	16
-22	1031	10		
-18	1026	9	1055	14
-11	1021	10		
-6	1020	8.0	1043	9.6
+6	1005	8.0	1030	7.2
+11	996	7.6	1018	
+17	990	6.6	1018	6.2
+30	976	5.8	1008	6.0
+37			1004	4.4
Date	October 30, 1975		November 5, 1975	

Table 29. Chemical Shift (Hz) of acid proton of acetic acid on different dates (of 1975) at Room Temperature

Sample	Chemical Shift (Hz) / Date					
30%	1042	1027	1020	1046	1048	1048
	July 17	Aug. 8	Oct. 12	Oct. 28	Oct. 30	Nov. 3
30% Cu	1042	1047	1045	1049		
	July 17	Oct. 12	Oct. 22	Nov. 3		
20%	1006	1017	1013	1008	1009	
	July 17	Oct. 9	Oct. 12	Nov. 3	Nov. 5	
20% Cu	997	956	1004	1004		
	July 17	Oct. 12	Nov. 3	Nov. 5		
10%	938	942	944			
	July 17	Oct. 16	Nov. 3			
10% Cu	931	939	937			
	July 17	Oct. 10	Nov. 3			
40%	1067	1067	1065			
	July 17	Oct. 12	Oct. 22			
40% Cu	1065	1070	1070			
	July 17	Oct. 12	Oct. 15			
5%	858					
	Oct. 22					
15%	983					
	Oct. 22					
100%	1174					
	Oct. 22					

Table 30. Time: July 17, 1975; Temp: 37°C

Proton	10%	10% Cu	20%	20% Cu	30%	30% Cu	40%	40% Cu
Position (Hz)								
HAc	938	931	1006	997	1042	1042	1067	1065
CH_3COOH	212	215	213	215	213	215	213	214
CH_3CN	208	207	208	206	208	208	207	207
Line Width (Hz)								
HAc	11	13	5.6	6.0	3.8	6.0	4.6	4.2
CH_3COOH	1.7		1.4	6.0	1.4	6.5	3.0	6.5
CH_3CN	3.7	3.6	3.5	3.3	3.2	6.0	4.0	4.2

Table 31. Time: October 12, (5% and 15% were run on Oct. 22); Temp: 37°C

Proton	5%	15%	20%	20% Cu	30%	30% Cu	40%	40% Cu
HAc	858	983	1013	956	1020	1047	1067	1070
CH_3COOH			210	214	212	213	210	213
CH_3CN			206	207	208	204	204	205
HAc	48	5.8	3.6	7.4	3.0	2.6	2.	2.2
CH_3COOH	1		0.9	8.5	1.5	5.5	1.3	4.5
CH_3CN	1		1.3	1.3	1.8	1.5	1.5	1.5

Table 32. Time: July 22, 1975; Temp: $-32^{o}C$

Sample	HAc		CH_3COOH		CH_3CN	
	C.S.(Hz)	L.W.(Hz)	C.S.(Hz)	L.W.(Hz)	C.S.(Hz)	L.W.(Hz)
40%	1133	7.6	208.5	3.1	203	2.7
40% Cu	1131	11.	207	5.0	202	3.5
30%	1107	11	209	2.4	204	2.5
30% Cu	1106	12	207	6.0	202	3.1
20%	1092	20	208	3.0	203	3.1
20% Cu	1070	19	208	6.0	202	3.1

Table 3.3 Time: July 22, 1975; Temp: $-40^{\circ}C$

Sample	HAc C.S.(Hz)	L.W.(Hz)	CH_3COOH C.S.(Hz)	CH_3CN C.S.(Hz)
40%	Frozen			
40% Cu	1146		209	204.5
30%	1125	18.	210	206
30% Cu	1121	18.8	208	203
20%	1100	29	208.5	204.5
20% Cu	1082	28	209	204
10%	1040	64	210.5	205
10% Cu	1026	58	211	204

Table 34. Temperature relationship between methanol shift, our variable temperature accessory regulator reading, ^{o}C, and 1000/T

Methanol shift	Regulator reading	^{o}C	1000/T
225	-40	-56.5	
217	-30	-45.2	4.4
211	-25	-40	4.3
208	-20	-36.2	4.22
204	-15	-31.7	4.15
200	-10	-27	4.07
196	-5	-22	3.98
193	0	-18.5	3.92
186.5	5	-10.8	3.82
182.5	10	-6	3.745
177	15	0.5	3.66
172.5	20	5.5	3.58
168	25	11	3.52
163	30	16.5	3.45
159	35	21.5	
152	40	29.8	3.3
	55	37.1	3.226

APPENDIX C

OPTICAL SPECTROPHOTOMETRIC MEASUREMENTS

In Table 35 we list the results for different solutions.

Table 35. Spectra data for .005 M copper acetate in various solution at 24.5°C

Solution	$\varepsilon(\lambda)$ at 6900Å	$\varepsilon(\lambda)$ at 14100Å
100% HAc	.554	
40% HAc/CH_3CN	.638	0
40% + 4.4MH_2O	.496	1.13
30%	.631	0
20%	.639	0
20% + 3.354MH_2O	.511	.860
10%	.640	0
10% + 2.78MH_2O	.580	.713
0%	.70	.034

To determine the copper acetate dimer/monomer equilibrium in solution, we need to know the molar absorptivities $\varepsilon(\lambda)$ at 6900 Å, where the dimer has an absorption maximum and the dissociation products absorb little, and the procedure which follows Howald and Chang[26] is as follows:

For 3.5 g 10% HAc/CH_3CN with 0.005M $Cu_2(OAc)_4.2H_2O$ and .2ml H_2O

$.580/.3\ .005 = 386;\ 640/.3\times.005 = 426.67\ M^{-1}$

Dimer Fraction: $(386-70)/(426.67-70) = .885$

$$Cu_2(OAc)_4 + 4H_2O \rightleftarrows 2Cu(OAc)_2\cdot(H_2O)_2 \qquad \varepsilon = 35$$

$C_D = .005M \times (.885) = .00442M$

$C_M = (.00058M) \times 2 = .00116M$

$C_{H_2O} = X_1(.713)$

$3.5g = (.7856)(.9V) + (1.0491)(.1V),\ V = 4.3106\ ml$

$C_{H_2O} = (.2)(.998)(10^3)/(18)(4.3) = 2.578M$

$X_1 = 3.62$

For 2.89 g 20% HAc/CH_3CN with .005M $Cu_2(OAc)_4.2H_2O$ and $200\lambda H_2O$

$.511/(.3)(.005) = 340.7;\ .639/(.005)(.3) = 426\ M^{-1}$

Dimer Fraction: $(340.7-70)/(426-70) = .76$

$C_D = .005(.76) = .0038$

$C_M = (.0012)(2) = .0024$

$C_{H_2O} = X_2(.860)$

$2.89g = (.7856)(.8V) + (1.0491)(.2V)\quad V = 3.45\ ml$

$C_{H_2O} = .2(.998)\ (10^3)/(18)(3.45) = 3.216M$

$X_2 = 3.75$

For 2.07g 40% HAc/CH_3CN with .005M $Cu_2(OAc)_4.2H_2O$ and 200 λ H_2O

$.494/(.3)(.005) = 329.3M^{-1}$; $.638/(.3)(.005) = 425.3M^{-1}$

Dimer Fraction: $(329.3-70)/(425.3-70) = .73$

$C_D = .005(.73) = .00365$

$C_M = .00135(2) = .0027$

$C_{H_2O} = X_3(1.13)$

$2.07g = .7856(.6V) + 1.0491(.4V)$, $V = 3.32$ ml

$C_{H_2O} = .2(.998)(10^3)/(18)(2.32) = 4.78M$

$X_3 = 4.20$

Average the above X values, we get $\bar{X}_M = (X_1 + X_2 + X_3)/3 = 3.90$

For 10% HAc with Cu; $C_{H_2O} = 3.9(.713) = 2.781M$

$K = (C_M^2)/C_D\ (C_{H_2O})^4 = .0000049$

For 20% HAc with Cu; $C_{H_2O} = 3.9(.860) = 3.354M$

$K = C_M^2/C_D(C_{H_2O})^4 = .0000117$

For 40% HAc with Cu; $C_{H_2O} = 3.9(1.13) = 4.4M$

$K = C_M^2/C_D(C_{H_2O})^4 = .0000052$

Howald and Cheng reported K' = .03245 for $K' = C_M^2/C_D a^4_{H_2O}$ in acetic acid. Since at 2M H_2O the activity of water is .2083 we can write

approximately

$$C_{H_2O} = .1042\ C_{H_2O}$$

Therefore

$$K' = .03245 = \frac{C_M^2}{C_D(.1042)^4\ C_{H_2O}^4}$$

and

$$K = \frac{C_M^2}{C_D\ C_{H_2O}^4} = K'(.1042)^4 = 3.82 \times 10^{-6}$$

this corresponds to $K = C_M^2/C_D(C_{H_2O})^4 = 3.82 \times 10^{-6}$ which is quite close to the range of values observed here for acetic acid-acetonitrile mixtures

$(1.0415)^4 = 1.1766$

$.03245(.10415)^4 = .03818 \times 10^{-4}$

APPENDIX D

DISCUSSION OF THEORY SELECTED AND ADAPTED FROM THE REFERENCES

Copper, $3d^{10}4s^{1}$

Copper is the transition element of the first series which has a single s electron outside the filled 3d shell. It can not be classed in Group I, since it has little in common with alkalies except formal stoichiometries in the +1 oxidation state. The filled d shell is much less effective than a noble-gas shell in shielding the s electron from the nuclear charge, so that the first ionization potential of Cu is higher than those of the alkalies. Since the electrons of the d shell are also involved in metallic bonding, the heat of sublimation and the melting point of copper are also much higher than those of the alkalies. These factors are responsible for the more noble character of copper, and the effect is to make the compounds more covalent and to give higher lattice energies, which are not offset by the somewhat smaller radius of the unipositive ion compared to the alkali ions in the same period - Cu^{+}, 0.93; Na^{+}, 0.95; and K^{+}, 1.33 Å. The second and third ionization potentials of Cu are very much lower than those of the alkalies and account in part for the transition-metal character shown by the existence of colored paramagnetic ions and complexes in the II and III oxidation states. The dipositive state is the most important one for copper, most cuprous compounds are fairly readily oxidized to cupric compounds, but further oxidation to Cu^{III} is difficult. There is a well-defined aqueous chemistry of

Cu^{++}, and a large number of salts of various anions, many of which are water-soluble, exist in addition to a wealth of complexes. Compounds and complexes of Cu^{++} are paramagnetic with one unpaired electron.

Stereochemistry (Jahn-Teller Effect) of Cu (II)

In 1937 Jahn and Teller proved that a nonlinear polyatomic molecular system in a degenerate electronic state will be unstable and will undergo some kind of distortion that will lower its symmetry and split the degenerate state. This theorem has great practical importance in understanding the structural chemistry of certain transition-metal ions. According to the Jahn-Teller theorem, distortions are to be expected in an octahedral complex of an ion with the configuration $t_{2g}^{6} e_{g}^{3}$. Therefore, the d^{9} configuration Cu makes Cu(II) subject to a Jahn-Teller distortion.

Ligand Field Theory of Cu(II) Complexes

For the elements of the first transition series, the use of ligand field theory in explaining both the spectra and magnetic properties of compounds has been far more extensive than their heavier congeners of the second and third transition series. Ligand field theory can be defined as the theory of (1) the origin and (2) the consequences of the splitting of inner orbitals of ions by their chemical environments. The inner orbitals of usual interest are partly filled ones, i.e., d or f orbitals.

The complexing of a metal ion to 6 equivalent and identical ligands leads to octahedral geometry and a molecule belonging to point group O_h. The octahedral arrangement which minimizes the mutual repulsions of the six-coordination is most readily pictured by placing the ligands at the plus and minus ends of the three coordinate axis. In the xy plane, the positions of such ligands relative to the d orbitals is shown in Figure 12_a while the corresponding diagrams for the xz and yz planes are shown in Figure 12_b and c. In the xy plane, the orbital d_{xy} lies between the ligands while $d_{x^2-y^2}$ points directly at the ligands. The latter orbital is therefore most affected by the ligand field and is raised in energy relative to the former. In a similar manner, in the xz plane, d_{z^2} is raised relative to d_{xz} and it is also raised relative to d_{yz} as the figure for the yz plane shows. If the alignments of the three orbitals, d_{xy}, d_{xz} and d_{yz}, relative to the ligands are compared, it will be seen that these are identical. It follows that in the full three-dimensioned case, these three orbitals are identical in energy and are stabilized relative to the other two. It is found by more detailed calculation, that the remaining orbitals, d_{z^2} and $d_{x^2-y^2}$, are also identical in energy and are destabilized. The combined energy level diagram is therefore composed of two upper orbitals, of equal energy, and three lower orbitals, which are also degenerate (Fig.13). The energy zero is conveniently taken as the weight mean of the energies of these two sets of orbitals; the

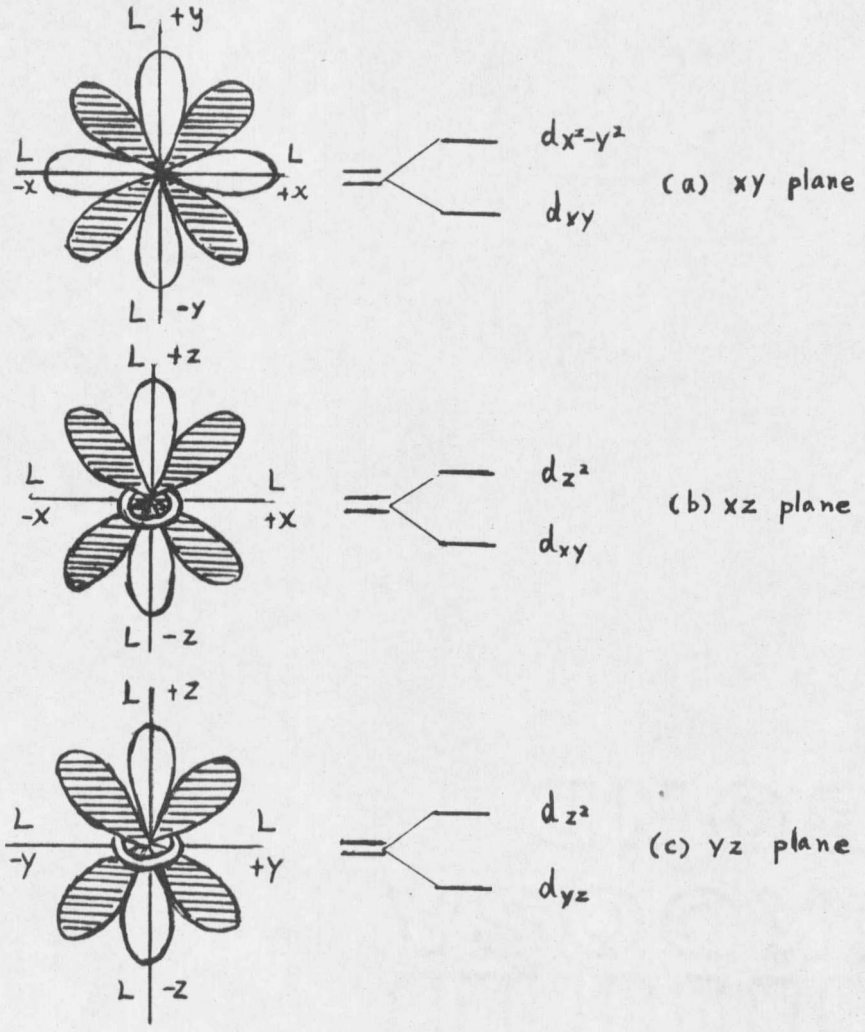

Figure 12. Positions of ligands and d orbitals in an octahedral complex: (a) the xy plane, (b) the xz plane, (c) the yz plane. (The d_{xy}, d_{yz}, and d_{zx} orbitals are indicated by shading.)

lower trio are thus stabilized by -2/5 ΔE while the upper pair are destabilized by 3/5 ΔE, where ΔE is the total energy separation.

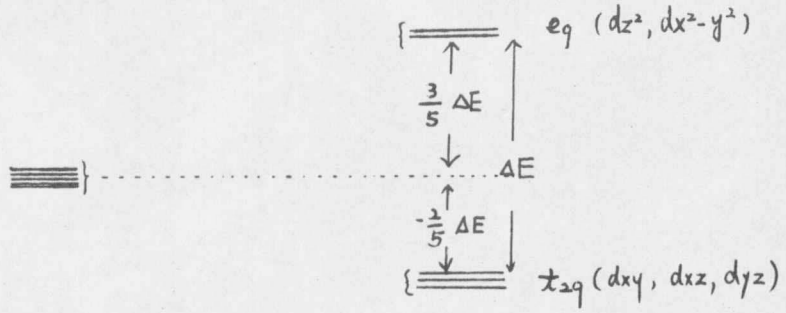

Figure 13. Energy level diagram for the d orbitals in an octahedral field

From the above octahedral complex, MX_6, if we slowly withdraw two trans ligands, we can get the pattern of splitting of the d orbitals in tetragonally distorted octahedral complexes. Let these be the two on the z-axis. As soon as the distance from M^{m+} to these two ligands becomes greater than the distance to the other four, new energy differences among the d orbitals arise. First of all, the degeneracy of the e_g orbitals is lifted, the z^2 orbital becoming more stable than the (x^2-y^2) orbital. This happens because the ligands on the z-axis exert a much more direct repulsive effect on a d_{z^2} electron than upon a $d_{x^2-y^2}$ electron. At the same time the three-fold degeneracy of the t_{2g} orbitals is also lifted. As the ligands on the

z-axis move away, the yz and zx orbitals remain equivalent to one another, but they become more stable than the xy orbital because their spatial distribution makes them more sensitive to the charges along the z-axis than is the xy orbital. Thus, for a small tetragonal distortion of the type considered, we may draw the energy level diagram shown in Figure 14.

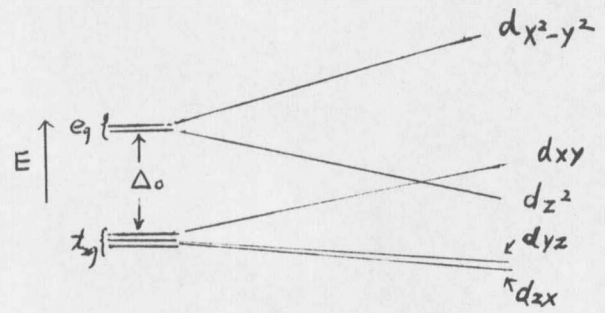

Figure 14. Energy-level diagram showing the further splitting of the d orbitals as an octahedral array of ligands becomes progressively distorted by the withdrawal of two trans-ligands, specifically those lying on the z-axis

As Figure 14shows, it is in general possible for the tetragonal distortion to become so large that the z^2 orbital eventually drops below the xy orbital. Whether this will actually happen for any particular case, even when the two trans-ligands are completely removed so that we have the limiting case of a square, four-coordinated complex, depends upon quantitative properties of the metal ion and the ligand

concerned. Seme-quantitative calculations with parameters appropriate for square complexes of Co^{II}, Ni^{II} and Cu^{II} lead to the energy-level in which the z^2 orbital has dropped so far below the xy orbital that it is nearly as stable as the (yz, zx) pair. As Figure 3 indicates, the d_z2 level might even drop below the (d_{xz}, d_{yz}) levels and, in fact, experimental results suggest that in some cases (e.g., $PtCl_4^{2-}$) it does.

Metal-to-Metal Bonds and Metal Atom Clusters

Transition metals have a marked propensity to form homo- and hetero-nuclear bonds among themselves. Structurally, compounds containing metal-to-metal (M-M) bonds may be divided into two broad classes: (1) those with only two-center bonds, which may, however, be of multiple character[2], and (2) those containing three or more metal atoms, like or unlike, arranged in a polygonal or polyhedral array with, in some cases, considerable delocalization of the bonding electrons. The length of a bond of given multiplicity between a given pair of metal atoms is a sensitive function of oxidation states, nature of additional ligands and other aspects of the molecular structure, and the use of interatomic distances to infer the existence and strength of metal-metal bonds requires caution. Two types of binuclear system in which M-M interactions can run the gamut from very

strong and multiple to weak or even entirely repulsive are shown in Fig. 15.

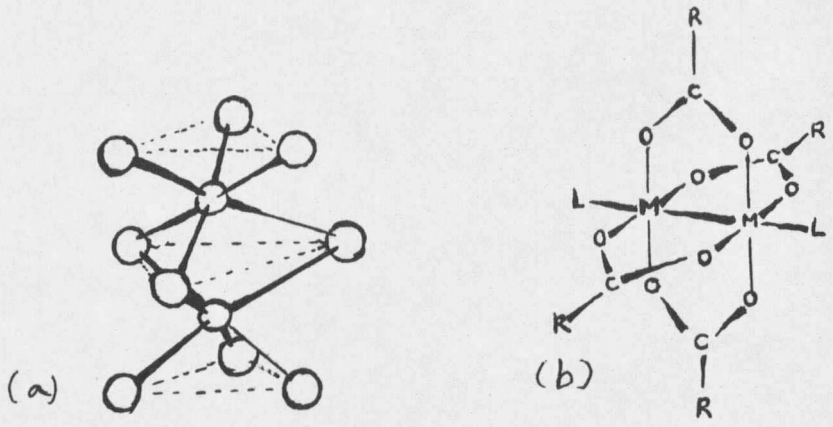

Figure 15. Two types of structure in which a full range of M-M interaction from strongly bonding to net repulsive can be observed (a) the confacial bioctahedron (b) the carboxylato-bridged dinuclear molecules

As to the factors favoring M-M bonding, the most important single factor appears to be low formal oxidation state. In order to attain a sufficient overlap of the metal valence-shell orbitals at distances that do not introduce too much repulsive interaction of the cores, the formal charge has to be low, thus permitting expansion of the valence shell orbitals. A second factor is the suitability of the valence-shell configuration and the metal-ligand bonding system.

The Nature of the Copper-Copper Bond in Copper (II) Acetate

In 1915, Lifschitz and Rosenbohm[3] recorded that the molar susceptibility of copper (II) acetate monohydrate at room temperature is much lower than that usually observed for copper (II) compounds. Many investigators have repeated these magnetic measurements, and its abnormally low magnetic moment has been established.[4] In 1951, Guha[5] found that the magnetic susceptibility of its hydrate passes through a maximum at near 270°K, and decreases rapidly as the temperature is lowered, not obeying the Curie-Weiss law. In 1951-1953, the anomalous behavior or its paramagnetic resonance spectrum was observed by many investigators.[6-11] The spectra resemble those of an ion of spin 1 rather than spin ½ which is present in most ordinary copper (II) compounds. Furthermore, the intensity decreases as the temperature is lowered in agreement with Guha's result of the temperature variation of susceptibilities. Bleaney[9] considered the isolated pairs of copper (II) ions must interact through exchange forces of Kramer's superexchange type.[12,13] In 1953, Niekerk and Schoenning[14,15] determined the crystal structure of copper (II) acetate monohydrate. It consists of a binuclear molecule $Cu_2(CH_3COO)_4 \cdot 2H_2O$ in which copper (II) ions are bridged in pairs by four acetate groups with two water molecules occupying the terminal positions (Figure 16). The copper (II) ion is 0.22 Å out of the plane of the four oxygen atoms, Cu-Cu, 2.64 Å; Cu-O,

1.97 Å; and Cu-OH_2, 2.20 Å. The striking feature of this six-fold coordinated copper complex is the close approach of 2.64 Å between the two copper (II) ions which is only slightly greater than 2.56 Å, the interatomic distance in metallic copper. In 1956, exact measurement of the temperature variation of the magnetic susceptibilities of anhydrous and hydrated copper (II) acetates were performed by Figgis and Martin[16] and Perakis[17] for the purpose of obtaining more information about the nature of the copper-copper bond in the acetates. Figgis and Martin's discussion will be described briefly in the following.

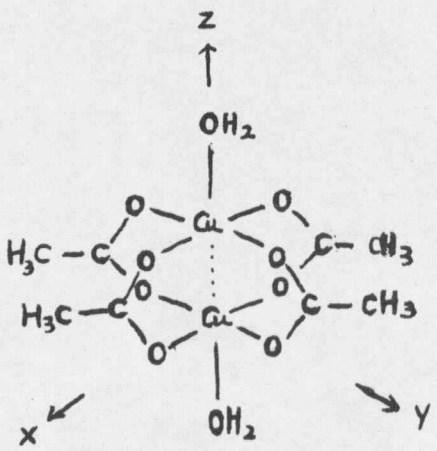

Figure 16. Schematic expression of the structure of $Cu_2(CH_3COO)_4.2H_2O$ molecule

The molar susceptibility, χ_M, is expressed as

$$\chi_M = \frac{g^2 N\beta^2}{3kT} \left(1 + \frac{1}{3} e^{J/KT}\right)^{-1} + N\alpha \qquad (3)$$

where g is the magnetic field splitting factor which is 2 if the magnetic moment arises from spin only, J is the exchange integral of magnetism theory, and N_α is the temperature independent paramagnetism of 1 mole of copper (II) ions.[18,9,16] The curves of X_M obtained by experiment coincide well with those based on Eq. 3 (cf. Figure 17). It has a definite maximum at a certain temperature, an indication of the antiferromagnetism of the substance.

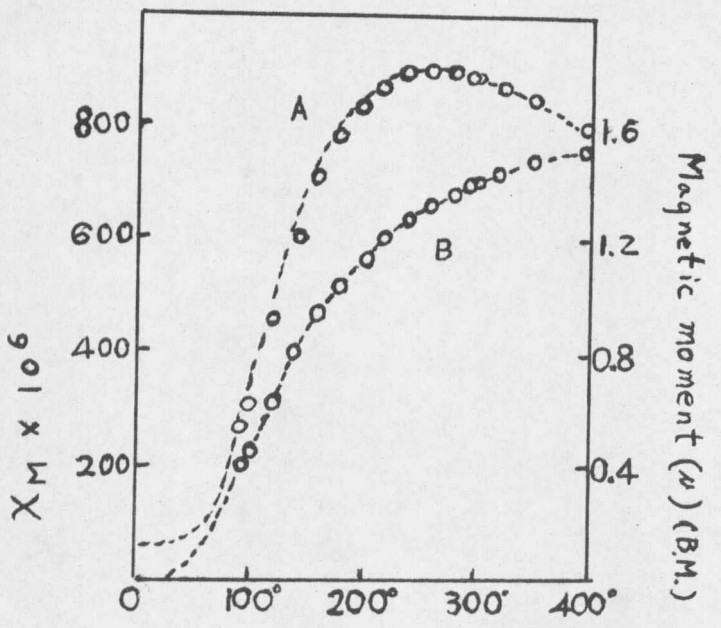

Figure 17. Magnetic susceptibilities (χ_M) and magnetic moments (μ) of copper (II) acetate monohydrate; --------, theoretical curves: curve A, magnetic susceptibilities; curve B, magnetic moments; 0, experimental values

J-values were calculated by inserting the measured χ_M values into Eq. 1; J = 302 cm^{-1} for the monohydrate. The sign of J indicates that the molecular triplet state lies above the singlet ground state (antiferromagnetism). The distance between the two states corresponds to J.

In 1962, Forster and Ballhausen[19] considered the electronic structure of the dimeric copper acetate in terms of molecular orbital theory (Figure 18). The important point of their treatment lies in the assumption of a large overlap between $3d_z2$ orbitals so that the antibonding level from the $3d_z2$ molecular orbitals has a higher energy than that of the molecular orbitals from $3d_{x^2-y^2}$. They proposed that a rather strong σ-bond ($3d_z2$ - $3d_z2$) between the two copper units, instead of the weak δ-bond proposed by Figgis.[16] In their treatment, the antiferromagnetism of copper (II) acetate is produced by the singlet $^1A_{1g}$ → triplet $^3B_{1g}$, corresponding to a one electron transition from the antibonding level of the $3d_{x^2-y^2}$ molecular orbitals to that of the $3d_z2$ molecular orbitals, or vice versa. They succeeded in part to explain consistently the experimental features of antiferromagnetism, absorption spectrum and g-factors. However, in 1968 Bose, Bagchi and Sen Gupta[20] interpreted the exchange interaction coefficient (J), spectroscopic splitting factors and magnetic susceptibilities, on the basis of C_{2v} symmetry for electronic states of each half of the complex. With the assumption of C_{2v} symmetry they found

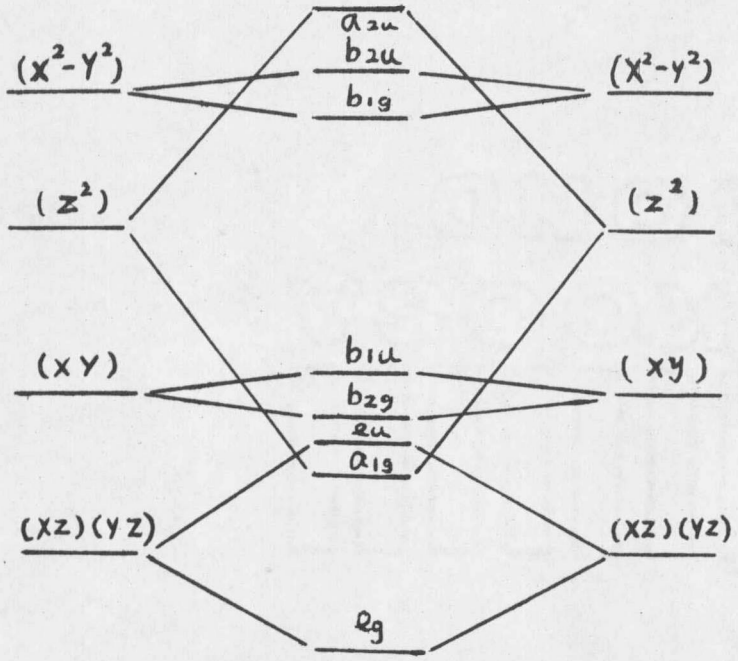

Figure 18. Highest molecular orbitals for $Cu_2(OAc)_4.2H_2O$. Not drawn to scale. Point group symmetry D_{4h}.

that the bonding between two halves of the complex is a mixture of σ or δ-type instead of pure σ or δ-type as obtained with the assumption of C_{4v} symmetry. The complete explanation of the nature of the copper-copper bond is still an interesting unsolved problem.

Dimer/Monomer Equilibrium of Copper (II) Acetate

Hydrated copper (II) acetate $Cu_2(CH_3COO)_4.2H_2O$ crystallizes with the copper ions arranged in pairs. In acetic acid and many other solvents, the copper acetate is also mainly in the dimeric form[21-26]

with only small dissociation to monomers ($CuAc_2$ with solvent ligands) and very few free ions ($CuAc^+$ and Cu^{++}). A Cu^{++} ion lacks one electron in the 3d shell. Hence, it has a magnetic moment with $s = \frac{1}{2}$, and optical transitions are possible between the 3d states, if the ion is in an asymmetric environment. The dimer-monomer dissociation of copper acetate in solutions can be determined, since the copper pair structure influences the magnetic and optical properties in the following way: In solvated $CuAc_2$, $CuAc^+$, and Cu^{++}, the copper ion is surrounded by a somewhat distorted octahedron of 6 neighboring negative ions giving an electrostatic field of mainly cubic symmetry on the copper site. In the dimer, however, each copper ion "sees" a field, where the inversion symmetry is destroyed by the presence of the other Cu^{++} as a nearest neighbor. Therefore, the copper acetate dimers show considerably stronger optical absorption than the dissociated species, and the absorption peaks are shifted slightly in frequency. While octahedrally coordinated Cu^{2+} ions in water show vibrationally allowed absorption around 8000 Å with molar extinction coefficient $\varepsilon \approx 10$, the dimer spectrum is similar to that of copper acetate crystals, which have a strong line at 7000 Å ($\varepsilon \approx 200$), with a shoulder at 9000 Å ($\varepsilon \approx 50$). There have been many attempts to interpret the dimer spectrum.[27-34] The X-ray structure of copper acetate and the difference between g_x and g_y show that the local symmetry in the solid, as seen by the Cu^{++} ion, is not higher than C_{2v}. The

polarization of the absorptivity then favors the assignment proposed by Kokoszka et al.[33] in the hole formalism: ground state $d_{x^2-y^2}$; transitions at 7000 Å to states d_{xz} and d_{yz}; and at 9000 Å to state d_{xy}. Kokoszka et al. also assigned the 3700 Å transition to the d_{zz} state, but it is more likely that this transition involves ligand orbitals (charge transfer) or Cu-Cu interactions. The transition to d_{xy} is allowed only in the lower symmetry group C_2. The crystal 9000 Å line is weak at room temperature, but much stronger at 77°K which indicates a greater distortion of the lattice at low temperature.

NMR and the Study of Ligand Substitution Process

General remarks. In the study of rates and mechanisms of substitution of one ligand of a coordination compound by another, a solvent molecule is almost inevitably a participant, either as the entering ligand or as the leaving ligand. This situation brings into the foreground reactions of the type:

$$MS_6 + S^* = MS_5S^* + S$$

Where M is a metal, S is the solvent, and the asterisk marks an artificial (often experimentally entirely meaningless) distinction between solvent molecules.

The reaction is an exchange process for which no net chemical change occurs. Since nuclear magnetic resonance absorption (n.m.r.) line shapes depend upon molecular dynamic processes which may include the exchange of nuclei between chemically inequivalent sites, a powerful tool was brought to bear on the exchange reaction problem. This tool is not limited by the requirements of chemical separation and has been applied to ligand exchange processes with rate constants up to 10^{+9} sec^{-1}. Whether or not a particular rate can be measured depends on a comparison between the desired rate and the rate of one or more of several possible relaxation processes. In different

situations, relaxation times may vary as much as eight powers of ten. Each type of reacting system must be considered as a separate case. Under certain conditions it is possible to determine the rate of the transfomation by its effect upon lineshape.[37]

Coalescence temperature. In a molecule, protons of two non-equivalent sets will show two lines in the n.m.r. spectrum, when the rate of exchange of protons between the two environments is very slow. Each line comes from one set of protons. As the temperature is raised, the exchange becomes rapid enough to affect the spectrum. At first, the lines are simply broadened. At greater exchange rates, the two lines merge into a single broad line. This temperature is called the coalescence temperature. At higher temperatures the line becomes narrower until a limit is reached where further increases in the exchange rate have no effect on the spectrum. The position of the single merged line will be a weighted average of the position of the original lines.

Bloch equations. A simple and straightforward treatment of the n.m.r. absorption is based on the Bloch phenomenological equations for the magnetization of the sample.[35] These equations are well presented in Stengle and Lungford,[36] "NMR in Ligand Substitution Reactions." Their treatment, slightly adapted, is given in this section.

A magnetization, M, is induced within a sample when it is in a magnetic field, H_o. The motion of M under an applied radiofrequency field, H_1, gives an observed n.m.r. spectrum. The Bloch equations are a set of three differential equations which give the variation with time of the three components of the vector M. M_z is taken along the direction H_o, and its direction is called the longitudinal direction. The other two components are in a plane perpendicular to H_o and M_z. The radiofrequency field is also applied in this plane. Since the components in this plane vary sinusoidally with time, variables u and v are defined as the transverse components of the magnetization which are in phase and 90° out of phase with the impressed radiofrequency field H_1. This definition is the same as to take the transverse components of M with respect to a coordinate system rotating at the frequency of H_1 instead of using a set of laboratory fixed axis. In the rotating coordinate system, the Bloch equations are:

$$dM_z/dt = \gamma H_1 v - (M_z - M_0)T_1 \qquad (4\text{-a})$$

$$dv/dt = -\gamma H_1 M_z + (\omega_o - \omega)u - v/T_2 \qquad (4\text{-b})$$

$$du/dt = -(\omega_o - \omega)v - u/T_2 \qquad (4\text{-c})$$

Where ω° is the frequency of precession of the nucleus, ω is the frequency of the radiofrequency field, γ is the magnetogyric ratio of the nucleus, and T_1 and T_2 are the longitudinal (spin-lattice) and transverse (spin-spin) relaxation times respectively. Equation 4-a shows

that the conduct of M_z is the result of two opposing processes. The first term on the right shows the interaction between M and H_1, this makes M_z depart from its equilibrium value. The second term considers the effect of spin-lattice relaxation which causes M_z to decay back to its equilibrium value, M, with a time constant T. Equations 4-b and 4-c result from similar considerations. The last term in these equations describes the tendency of u and v to decay to their equilibrium values of zero with a time constant T_2. The microscopic interpretation of T_2 can be made if we consider a sample as a collection of nuclear magnets (spins) which are precessing about the H_o direction. If all of them are moving in phase, the projections of their moments onto the xy plane will be parallel and add up to a finite value for M_{xy}, which will result in nonzero values for u and v. In the absence of outside influences, different processes cause the spins to get out of phase with one another over a period of time. When the phases are completely randomized, u and v will be zero. This process is spin-spin relaxation.

If we sweep through the spectrum slowly, the steady state conditions apply. The magnetization of the sample changes slowly, and the time derivatives in the Bloch equations may be set equal to zero. The two opposing tendencies; the effect of relaxation processes which dephase the spins, and the effect of H_1 in bringing spins together; will give a signal. The above opposition causes the absorption of

energy to take place over a range of frequencies, giving the n.m.r. line a definite width which is related to T_2.

Gutowsky, McCall, and Slichter,[38] and McConnell[39] first included the possibilities of chemical exchanges between two sites A and B, by setting down the differential equations for the protons of type A and then adding two terms, one of which includes the effect of A type magnetization disappearing as A protons are converted into B protons, the other accounts for the appearance of A type magnetization as B protons are converted into A. Finally, they obtained a total of six equations, three for each type of proton. This has been given in several texts.[37] It is more convenient to divide the results of the analysis into several categories depending on the magnitude of the exchange rate, and to discuss each one separately.

If we consider a system where the spectrum consists of two isolated narrow lines unmodified by chemical exchange, their line widths will be easily measured. From the unmodified Bloch equations, the line widths (in this paper, the full line width at half height) in cycles per second are related to the transverse relaxation times T_2 by:[35]

$$\Delta\nu_A = 1/\pi T_{2A};\ \Delta\nu_B = 1/\pi T_{2B} \qquad (5)$$

Where A and B refer to the type of proton. The reciprocal of the transverse relaxation time is determined by the rate of physical

processes which cause the precessing nuclei to lose phase coherence with each other and hence cause the value of the transverse magnetization (u and v) to decay to zero in the absence of H_1. When chemical exchange between the two environments is slow but significant, the two lines are broadened slightly, and their widths can be described by the apparent relaxation times T'_{2A} and T'_{2B} where:

$$1/T_{2A}' = 1/T_{2A} + 1/\tau_A;\ 1/T_{2B}' = 1/T_{2B} + 1/\tau_B \qquad (6.)$$

τ_A and τ_B are the mean lifetimes of a proton in the environments A and B, respectively. These equations are for lines which are not so broad as to overlap. This condition is illustrated in the curve at -3.5 of Figure 19. This condition is the "slow exchange region" in which the line broadening has to be small compared to the line separation. Matwiyoff's[40] work on the Co^{II}-N,N-dimethylformamide system gives a good example of kinetic study in coordination chemistry using data from the slow exchange region. At quite low temperatues it was possible to distinguish two sets of dimethylformamide (dmf) signals in a solution of $Co(dmf)_6(ClO_4)_2$ in dmf. One of these was from dmf in the bulk dolvent and it is strong and relatively narrow; the other was from dmf molecules bound to the Co ion and it is broad and weak due to interaction with the paramagnetic ion. Three lines of this second set (corresponding to the three types of protons on dmf) were observed and their widths as a function of temperature are shown in Figure 20.

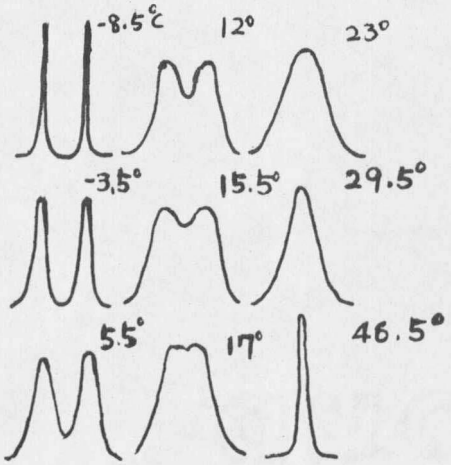

Figure 19. The proton magnetic resonance spectrum of pure liquid N,N-dimethyltrichloroacetamide (DMTCA) as a function of temperature at 60 MHz. The frequency scale, but not the intensity scale, is the same for all temperatures.

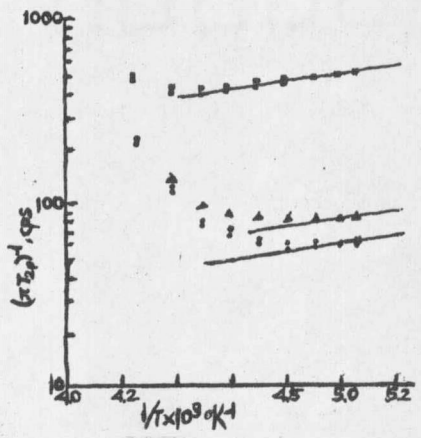

Figure 20. Temperature dependence of $(\pi T_{2M})^{-1}$ for the formyl and methyl protons in the complex $Co(dmf)_4^{2+}$.

At lower temperatures, the exchange of dmf molecules between sites was slow and there were no effect on the spectrum. The weak temperature dependence of the linewidth is due to the change of the relaxation time T_{2M} (M refers to the environment of the coordination sphere of a metal ion). At higher temperatures, τ_M^{-1} becomes significant, therefore the linewidth increases rapidly because of the strong temperature dependence of τ_M. Finally, at temperatures where 1/T (the reciprocal of the absolute temperature) is less than 0.0043, the separate signals from coordinated dmf can no longer be observed. In the intermediate temperature region of Figure 20 exchange rates can be calculated from Equation 6, and a straight line fitted to the temperature dependence yields the activation energy. Their results were in excellent agreement with values obtained from other data (vide infra).

The bulk solvent proton resonance of the acetonitrile-Ni^{II} system in Figure 21 is a similar system which has been studied over the full range of exchange rates. At low temperature, where exchange is negligible, the solvent proton linewidths show a very slight temperature dependence, the low temperature linewidths of bulk solvent protons are principally determined by long range interactions between the bulk solvent and the metal atom when the metal complex is paramagnetic; this is often called "second sphere broadening," and it depends upon factors similar to those entering into T_{2M}, this is illustrated in region I of Figure 21. When the exchange is fast enough to

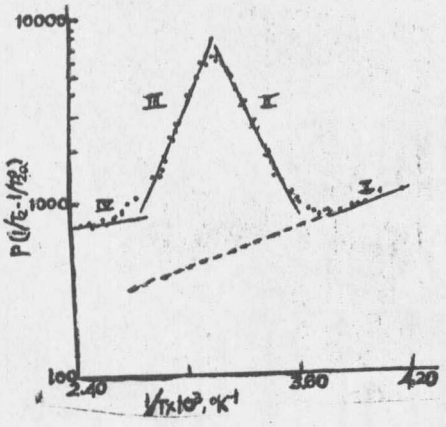

Figure 21. Temperature dependence of $(1/P_M)(1/T_2-1/T_{2A}^{\circ})$ for the protons in CH_3CN in solutions of $Ni(CH_3CN)_6^{2+}$ at 5 6.4 MHz

be significant, the linewidth increases rapidly with increasing temperature as shown by region II of Figure 21. Since the most accurate results may be obtained from this region, the exchange rate data are usually obtained here. The signal of bulk solvent protons is strong and its shape is very sensitive to the rate. The exchange rate is usually calculated from the expression:*

$$1/T_2 - 1/T_{2A}^{\circ} = 1/\tau_A = P_M/\tau_M \qquad (7)$$

Where the subscript A indicates the bulk solvent phase, and T_{2A}° is the relaxation time observed in the pure solvent. This equation ignores the effect of second sphere broadening. If we assume that the second sphere effects observed in region I can be extrapolated to high temperature, we get the dotted line of Figure 21. Since the linewidths in region II are closely related to τ_M, it is easy to calculate the activation parameters for the pseudo first order exchange reaction from Equation (8), and many solvent-metal ion systems have been analyzed using these expressions.

$$k_1 = 1/\tau_M = \frac{kT}{h} \exp[-\Delta H^{\neq}/RT + \Delta S^{\neq}/R] \qquad (8)$$

---

*It can be shown by detailed balancing that:

$$P_A = \frac{\tau_A}{\tau_A+\tau_M} \; ; \; P_M = \frac{\tau_M}{\tau_A+\tau_M}$$

Thus, for dilute solutions where P_M is small, $\tau_A^{-1} = P_M\tau_M^{-1}$.

Relaxation times in paramagnetic solutions. T_{2M} is much smaller than T_{2A} in solutions of paramagnetic ions, and a physical picture of the process leading to region II can be given. A solvent will have a relaxation time T_{2A} if there is no exchange, however, a second relaxation mechanism will become important if the average lifetime of a molecule in the bulk solvent between periods of being bound to a paramagnetic ion is short compared to T_{2A} (i.e., $\tau_A \ll T_{2A}$). Especially, if the solvent remains coordinated long enough for relaxation to occur, i.e., $\tau_M \gg T_{2M}$, it will be relaxed every time it enters that environment. This mechanism predominates when $\tau_A \ll T_{2A}$, and the relaxation time is the mean lifetime of the molecule in the bulk. Therefore, a solvent molecule spends most of its time in the bulk phase, and only occasionally bind to the metal for a brief period, and it is relaxed during this time. Coordination to the metal produces a paramagnetic pulse which alters the phase of the processing nucleus. In Figure 19 $T_{2A} = T_{2M}$, and the most important parameter is the chemical shift between the two environments, however, in the present case, which may be applied to the analysis of Figure 21, the difference in relaxation times (T_{2A} and T_{2M}) is paramount, and the same linewidth effects would be observed even if the chemical shift were zero.

Swift and Connick[42-46] have given a solution of the Bloch equations for the system which considers both the effects of a relaxation

time and a chemical shift, and their results have been used by all subsequent workers in this field as a guide line. For a solution which is dilute in the metal ion, the relaxation time is:

$$\frac{1}{T_2} - \frac{1}{T_{2A}} = \frac{P_M}{\tau_M} \frac{T_{2M}^{-2} + (T_{2M}\tau_M)^{-1} + \Delta\omega_M^2}{(T_{2M}^{-1} + \tau_M^{-1})^2 + \Delta\omega_M^2} \qquad (9)$$

Where T_2 is the experimentally observed relaxation time and $\Delta\omega_M$ is the chemical shift between bulk solvent and the coordination sphere of the metal. If the exchange is not too fast, we obtain the results discussed earlier with the additional point that the effect of the chemical shift is taken into account. This gives two possibilities: in one case the relaxation of the solvent nuclei in the paramagnetic environment is caused by the chemical shift; in the second case it is brought about by other factors. Since a nucleus at a metal ion will precess at a rate different from the nuclei in the bulk solvent, therefore a chemical shift will cause relaxation. The difference in precession rates will lead to dephasing of the two sets of nuclei, in a time τ_M, the phase difference will be $\tau_M\Delta\omega_M$. If the chemical shift is large, and τ_M is not too small, Equation 9 leads to:

$$\Delta\omega_M^2 \gg T_{2M}^{-2}, \tau_M^{-2}; \quad 1/T_2 - 1/T_{2A} = P_M/\tau_M \qquad (10)$$

When factors other than the chemical shift dominate the relaxation

process, we get the same result for the linewidth:

$$T_{2M}^{-2} >> \Delta\omega_M^2 \ \tau_M^2; \ 1/T_2 - 1/T_{2A} = \frac{P_M}{\tau_M} \qquad (11)$$

Therefore, the exchange rate can be determined regardless of the relaxation mechanism in this temperature region.

Linewidth changes with temperature as shown in regions III and IV of Fig. 21 result from rapid exchange rates. Here the lifetime in the coordination sphere is too short for relaxation to occur each time the solvent binds to the metal. Since several encounters between solvent and metal are required for relaxation, the linewidth is no longer directly proportional to the exchange rate. There are also two possibilities: effects due to chemical shift may predominate, or, if $\Delta\omega_M$ is small, terms depending on T_{2M} will be important. In the first situation we have:

$$\tau_M^{-2} >> \Delta\omega_M^2 >> (T_{2M}\tau_M)^{-1}; \ 1/T_2 - 1/T_{2A} = P_M\tau_M\Delta\omega_M^2, \qquad (12)$$

Since the linewidth depends upon τ_M, it will change rapidly with temperature, but in the opposite direction of region II.

In fast exchange region, the linewidth does not depend on the exchange rates, and it varies but slightly with temperature, this is the limiting high temperature region found in most systems in which the exchange rate is extremely fast. In this situation we have:

$$(T_{2M}\tau_M)^{-1} >> T_{2M}^{-2},\ \Delta\omega_M^2;\ 1/T_2 - 1/T_{2A} = P_M/T_{2M} \qquad (13)$$

Therefore, the stages of a typical experimental study are as following: first, the linewidth of the pure solvent is measured over a wide temperature range, then a solution of a paramagnetic ion is studied. The quantity log $P_M(1/T_2 - 1/T_{2A}^{\circ})$ is plotted vs. reciprocal temperature; the slope of the plot indicates which conditions apply, especially in view of the relatively large values of chemical activation energies. Sometimes, the exchange process is too fast to measure over the entire liquid range of the solvent, often this difficulty can be circumvented by taking as the probe nucleus the atom directly bound to the metal instead of a proton on the solvent (ligand) molecule. For this atom, $\Delta\omega_M$ is especially large, and T_{2M} is quite small. This conditions extend the applicability of Equations 10 through 12. Usually one is confident that the reaction is too fast to be in region I and calculates an apparent rate constant from Equation 10. If the conditions of region II apply, the true rate results. If the reaction is fast, and III or IV is appropriate, the experimental linewidth will be less than the linewidth expected for exchange rate control. Then the rate calculated from Equation 10 will be less than the true rate, in such studies, a lower limit for the exchange rate is usually reported.

LITERATURE CITED

LITERATURE CITED

1. (a) MacKay, K.M., and MacKay, R.A., Introduction to Modern Inorganic Chemistry.
   (b) Cotton and Wilkinson, Advanced Inorganic Chemistry.
   (c) Orchin Jaffe, Symmetry, Orbitals and Spectra.

2. Cotton, F.A., Rev. Pure Appl. Chem. (1967), 17, 25; Accounts Chem. Res., (1969), 2,240.

3. Lifschitz, J. and Rosenbohm, E., Z. Elektrochem., 21,499, (1915).

4. Figgis, B. N., and Martin, R. L., J. Chem. Soc., 3837 (1956).

5. Guha, B. C., Proc. Roy. Soc.(London), A206, 353 (1951).

6. Abe, H., and Shimada, J., J. Phys. Rev., 90, 316 (1953).

7. Bleaney, B., Rev. Mod. Phys., 25, 151 (1953).

8. Bleaney, B., and Browers, K. P., Phil. Mag., 43, 372 (1952).

9. _____, and _____, Proc. Roy. Soc. (London), A214, 451 (1952).

10. Kumagai, H., Abe, H., and Shimada, J., Phys. Rev., 87, 385 (1952).

11. Lancaster, F. W., and Gordy, W., J. Chem. Phys., 19, 1181 (1951).

12. Anderson, P. W., Phys. Rev., 79, 350 (1950).

13. Kramers, H., Physica, 1, 182 (1934).

14. Van Niekerk, J. N., and Schoening, F. R. L., Acta Cryst., 6, 227 (1953).

15. _____, and _____, Nature, 171, 36 (1953).

16. Figgis, B. N.m and Martin, R. L., J. Chem. Soc., 3837 (1956).

17. Perakis, N., Serres, A., and Karantassis, T., J. Phys. Radium, 17, 134 (1956).

18. Ballhausen, C. J., Introduction to Ligand Field Theory, McGraw-Hill Book Co., Inc., New York, NY (1962).

19. _____, Acta. Chem. Scand., 16, 1385 (1962).

20. Bose, A., Bagchi, R. N., and Sen Gupta, P., Indian J. Phys., 42, 55 (1968).

21. Tsuchida, R., Yamada, S., and Nakamura, H., Nature, 178, 1192 (1956).

22. Martin, R. L., and Whitley, A., J. Chem. Soc., 1394 (1958).

23. Kondo, M., and Kubo, M., J. Phys. Chem., 62, 468 (1958).

24. Kato, M., Jonassen, H. B., and Fanning, J. C., Chem. Rev., 64, 99 (1964).

25. Kochi, J. K., and Subramanian, R. V., Inorg. Chem., 4, 1527 (1965).

26. Cheng, A. T. A., and Howald, R. A., Inorg. Chem., 7, 2100 (1968).

27. Ross, I. G., Trans. Faraday Soc., 55, 1057 (1959).

28. _____, and Yates, J., Trans. Faraday Soc., 55, 1064 (1959).

29. Tonnet, M. L., Yamada, S., and Ross, I. G., Trans. Faraday Soc., 60, 840 (1964).

30. Hansen, A. E., and Ballhausen, C. J., Trans. Faraday Soc., 61, 631 (1965).

31. Boudreaux, E. A., Inorg. Chem., 3, 506 (1964).

32. Kokoszka, G. F., Inorg. Chem., 4, 1082 (1965).

33. _____, J. Chem. Phys., 42, 3693 (1965).

34. Bose, A., and Bagchi, R. N., Indian J. Phys., 42, 55 (1968).

35. Bloch, F., Phys. Rev., 70, 460 (1946).

36. Stengle, T. R., and Lungford, C. H., Coordin. Chem. Rev., 2, 349 (1967).

37. (a) Pople, J. A., Schneider, W. G., and Bernstfin, H. J., High-Resolution Nuclear Magnetic Resonance, (1959).
(b) Emsley, J. W., Feeney, J., and Sutcliffe, L. H., High Resolution Nuclear Magnetic Resonance Spectroscopy, (1965).
(c) Carrington, A., and McLachlan, A., Introduction to Magnetic Resonance, (1967).
(d) Allerhand, A., and Gutowsky, H. S., J. Chem. Phys., 41, 2115 (1964).

38. Gutowsky, H. S., McCall, D. W., and Slichter, C. P., J. Chem. Phys., 21, 279 (1953).

39. McConnell, H. M., J. Chem. Phys., 28, 430 (1958).

40. Matwiyoff, N., Inorg. Chem., 5, 788 (1966).

41. Ravage, D. K., Stengle, T. R., and Langford, C. H., Inorg. Chem., 6, 1252 (1967).

42. Swift, T. J., and Connick, R. E., J. Chem. Phys., 37, 307 (1962). See also crratum, J. Chem. Phys., 41, 2553 (1964).

43. Gutowsky, H. S., and Holm, C. H., J. Chem. Phys., 25, 1228 (1956).

44. Bernheim, R. A., Brown, T. H., and Gutowsky, H. S., J. Chem. Phys., 30, 950 (1959). Bloembergen, N., and Morgan, L. O., J. Chem. Phys., 34, 842 (1961).

45. Wayland, R. B., J. Am. Chem. Soc., 88, 4597 (1966); 88, 5600, (1966).

46. McConnell, H. M., and Chestnut, D. B., J. Chem. Phys., 28, 107 (1958).

47. Kaplan, J. I., J. Chem. Phys., 28, 278 (1958); 28, 462 (1958).

48. Alexander, S., J. Chem. Phys., 37, 974 (1962).

49. Kremann, R., Zoff, A., and Osward, V., Monatsh, 43, 139 (1922).

50. Davidson, D., and Skovronek, H., J. Am. Chem. Soc., 80, 379 (1958).

51. Durrell, W. S., Young, J. A., and Dresdner, R. D., J. Org. Chem., 28, 831 (1963).

52. (a) Krieble, V. K., and McNally, J. G., J. A. C. S., 51, 3368 (1929); (b) ibid., 60:2 2977 (1938).

53. Grasdalen, H., and Suare, I., Acta Chem. Scand., 25, 1081 (1971).

Dirks, Jennie L
Optical and proton magnetic resonance study of copper (II)

DATE	ISSUED TO